ATLAS CONF Note

ATLAS-CONF-2019-014

22nd May 2019

Searches for electroweak production of supersymmetric particles with compressed mass spectra in $\sqrt{s} = 13$ TeV pp collisions with the ATLAS detector

The ATLAS Collaboration

This note presents results of searches for electroweak production of supersymmetric particles in models with compressed mass spectra. The searches use 139 fb^{-1} of $\sqrt{s} = 13$ TeV proton-proton collision data collected by the ATLAS experiment at the Large Hadron Collider. Events with missing transverse momentum, two same-flavour, oppositely-charged, low transverse momentum leptons, and hadronic activity from initial state radiation are selected. The data are found to be consistent with predictions from the Standard Model. The results are interpreted using simplified models of R-parity-conserving supersymmetry in which the lightest supersymmetric partner is a neutralino with a mass similar to a chargino, heavier neutralino, or slepton. Lower limits on the masses of charginos in different simplified models range from 162 GeV to 205 GeV for moderate mass splittings, and extend down to mass splittings of 2 GeV to 2.6 GeV at the LEP chargino bounds. Similar lower limits on degenerate light-flavour sleptons reach up to masses of 256 GeV and down to mass splittings of 590 MeV.

ATLAS-CONF-2019-014
22 May 2019

1 Introduction

Extensions to the Standard Model (SM) that include new states with nearly-degenerate masses can help resolve problems in particle physics while evading constraints from colliders. The mass spectra of such new states are referred to in this paper as "compressed". In many models of Supersymmetry (SUSY) [1–6] one of the new particles produced in proton-proton (pp) collisions is assumed to be the lightest neutralino $\widetilde{\chi}_1^0$. In the compressed SUSY models considered in this paper, the $\widetilde{\chi}_1^0$ is close in mass to a heavier SUSY partner such as a chargino ($\widetilde{\chi}_1^\pm$), second-lightest neutralino ($\widetilde{\chi}_2^0$), or slepton ($\widetilde{\ell}$). If the $\widetilde{\chi}_1^0$ is stable, e.g. as the lightest SUSY partner (LSP) in R-parity conserving SUSY models [7], then it is a viable dark matter candidate [8, 9].

This note presents searches for physics beyond the SM in signatures sensitive to models with compressed mass spectra. Simplified SUSY models [10–12] are used to optimise the searches and interpret the results. The searches use 13 TeV proton–proton (pp) collision data corresponding to 139 fb^{-1} of integrated luminosity, collected by the ATLAS experiment [13] from 2015 to 2018 at the CERN Large Hadron Collider (LHC).

All searches assume pair production of SUSY particles via electroweak interactions, with subsequent decays to the $\widetilde{\chi}_1^0$ and SM particles. The neutralinos $\widetilde{\chi}_{1,2,3,4}^0$ and charginos $\widetilde{\chi}_{1,2}^\pm$ are collectively referred to as electroweakinos, where the subscripts indicate increasing electroweakino mass. These mass eigenstates are a mixture of wino, bino, and Higgsino fields[1] which form the SUSY partners of the SM W, γ/Z, and Higgs fields, respectively. In the minimal supersymmetric extension of the SM (MSSM) [14, 15], the masses of the bino, wino, and Higgsino states are parameterised by M_1, M_2, and μ, respectively. For large values of $\tan(\beta)$, these three parameters drive the phenomenology of the electroweakinos

Three SUSY scenarios are considered in the interpretation of the searches. In the first scenario, the lightest SUSY partners are assumed to be a triplet of Higgsino-like states ($\widetilde{\chi}_1^0$, $\widetilde{\chi}_1^\pm$, $\widetilde{\chi}_2^0$), in which the mass splitting between the states is partially determined by the magnitude of M_1 or M_2 relative to $|\mu|$. Such a scenario, referred to here as Higgsino models, is motivated by naturalness arguments [16, 17], which suggest that $|\mu|$ should be near the weak scale [18, 19] while M_1 and/or M_2 can be larger. The second scenario is similar to the first, except with $|M_1| < |M_2| \ll |\mu|$, so that the produced electroweakinos have wino and/or bino nature. In such wino/bino scenarios the LSP can be a thermal relic dark matter candidate that was depleted in the early universe through coannihilation processes to match the observed dark matter density [20, 21]. Such scenarios are also less constrained by dark matter direct detection experiments than Higgsino models [22]. Diagrams representing the production mode for the first two scenarios are shown in Figure 1(a). A $\widetilde{\chi}_2^0$ produced in either scenario can decay to a dilepton pair via an off-shell Z boson (Z^*), such that the dilepton invariant mass $m_{\ell\ell}$ is kinematically restricted to be smaller than the mass splitting between the $\widetilde{\chi}_2^0$ and $\widetilde{\chi}_1^0$. Hadronic initial-state radiation (ISR) is also required to boost the system as a way of enhancing the sensitivity of the search.

The third scenario assumes the presence of scalar partners of the SM leptons (slepton, $\widetilde{\ell}$) that are slightly heavier than a bino-like LSP. Such models can explain both dark matter thermal relic densities through coannihilation channels, as well as the muon $g-2$ anomaly [23, 24]. This process is illustrated in Figure 1(b). This scenario exploits the relationship of the leptons and the missing transverse momentum through the stransverse mass, m_{T2} [25, 26], which exhibits a kinematic endpoint similar to that for $m_{\ell\ell}$ in electroweakino decays.

[1] In the minimal supersymmetric extension of the SM the Higgs sector is extended to contain two Higgs doublets.

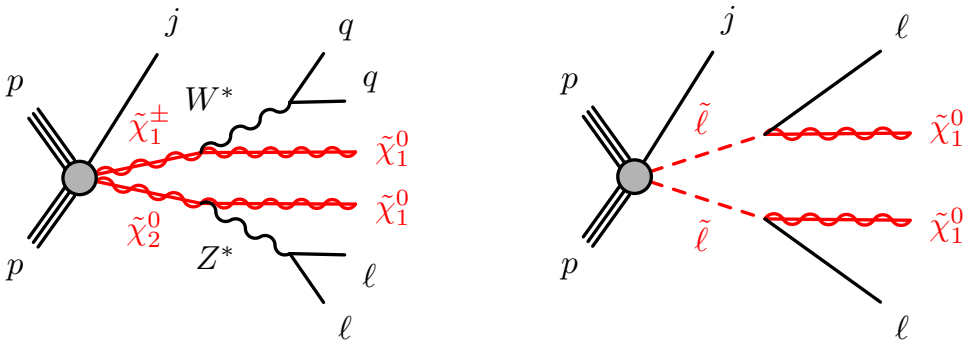

Figure 1: Diagrams representing the two-lepton final state of (a) production of electroweakino $\widetilde{\chi}_2^0\widetilde{\chi}_1^{\pm}$ with initial-state radiation (j), and (b) slepton pair $\widetilde{\ell\ell}$ production in association with initial state radiation (j). The Higgsino simplified model also considers $\widetilde{\chi}_2^0\widetilde{\chi}_1^0$ and $\widetilde{\chi}_1^+\widetilde{\chi}_1^-$ production.

Events with two same-flavour opposite-charge leptons (electrons or muons), significant missing transverse energy ($E_{\mathrm{T}}^{\mathrm{miss}}$), and hadronic activity are selected for all scenarios. Signal regions (SRs) are defined by placing additional requirements on a number of kinematic variables. The dominant SM backgrounds are either estimated with *in situ* techniques or constrained using data control regions (CRs) that enter into a simultaneous likelihood fit with the SRs. The fit is performed in bins of either the $m_{\ell\ell}$ distribution (for electroweakinos) or the m_{T2} distribution (for sleptons).

Collider constraints on these compressed scenarios were first established at LEP [27–37]. The lower bounds on direct chargino production from these results correspond to $m(\widetilde{\chi}_1^{\pm}) > 103.5$ GeV for $\Delta m(\widetilde{\chi}_1^{\pm}, \widetilde{\chi}_1^0) > 3$ GeV and $m(\widetilde{\chi}_1^{\pm}) > 92.4$ GeV for smaller mass differences, although the lower bound on the chargino mass weakens to around 75 GeV for models with additional new scalars and Higgsino-like cross sections [38]. For sleptons, conservative lower limits on the mass of the scalar partner of the right-handed muon, denoted $\widetilde{\mu}_R$, are approximately $m(\widetilde{\mu}_R) \gtrsim 94.6$ GeV for mass splittings down to $m(\widetilde{\mu}_R) - m(\widetilde{\chi}_1^0) \gtrsim 2$ GeV. For the scalar partner of the right-handed electron, denoted $\widetilde{e}_R$, LEP established a universal lower bound of $m(\widetilde{e}_R) \gtrsim 73$ GeV that is independent of $\Delta m(\widetilde{e}_R, \widetilde{\chi}_1^0)$. Recent papers from the CMS [39, 40] and ATLAS [41] collaborations have extended the LEP limits for a range of mass splittings. This note extends previous LHC results by increasing the integrated luminosity, extending the search with additional channels, and exploiting improvements in detector calibration and performance. The event selection was also reoptimised and uses techniques based on Recursive Jigsaw Reconstruction [42], which improve the separation of the SUSY signal from the SM backgrounds.

The rest of the note proceeds as follows. After a short description of the ATLAS detector, a summary of data and simulation samples used is presented. This is followed by descriptions of the event reconstruction, signal regions, background estimates, and systematic uncertainties. The results of the search are then presented, along with the interpretation of the results in the benchmark SUSY models. A brief conclusion is presented at the end.

2 ATLAS Detector

The ATLAS experiment is a general-purpose particle detector that surrounds the interaction point with nearly 4π solid angle coverage.[2] It comprises an inner detector, calorimeter systems, and a muon spectrometer. The inner detector provides precision tracking of charged particles in the pseudorapidity region $|\eta| < 2.5$, consisting of pixel and microstrip silicon subsystems within a transition radiation tracker. The innermost pixel detector layer, the insertable B-layer [43], was added for $\sqrt{s} = 13$ TeV data-taking to improve tracking performance. These are immersed in a 2 T axial magnetic field provided by a superconducting solenoid. High-granularity lead/liquid-argon electromagnetic sampling calorimeters are used for $|\eta| < 3.2$. Hadronic energy deposits are measured in a steel/scintillator tile barrel calorimeter in the $|\eta| < 1.7$ region. Forward calorimeters cover the region $3.2 < |\eta| < 4.9$ for both electromagnetic and hadronic measurements. The muon spectrometer comprises trigger and high-precision tracking chambers spanning $|\eta| < 2.4$ and $|\eta| < 2.7$, respectively, with a magnetic field provided by three large superconducting toroidal magnets. Events of interest are selected using a two-level trigger system [44], consisting of a first-level trigger implemented in hardware, which is followed by a software-based high-level trigger.

3 Data and Simulated Event Samples

Events were selected with a $E_{\mathrm{T}}^{\mathrm{miss}}$ trigger, employing varied trigger thresholds as a function of the data period, that is fully efficient for offline $E_{\mathrm{T}}^{\mathrm{miss}}$ values above 200 GeV for all periods. The dataset used corresponds to 139 fb^{-1}of $\sqrt{s} = 13$ TeV pp collision data, where the uncertainty on the integrated luminosity is 1.7%. It is derived from the calibration of the luminosity scale using x-y beam-separation scans, following a methodology similar to that detailed in Ref. [45], and using the LUCID-2 detector for the baseline luminosity measurements [46]. The average number of interactions per bunch-crossing was 33.7.

Samples of Monte Carlo (MC) simulated events are used to estimate the signal yields, and for estimating the background from process with prompt leptons, as well as in the determination of systematic uncertainties. For the first signal scenario, samples were generated for the Higgsino simplified model production of $\tilde{\chi}_1^- \tilde{\chi}_1^+$, $\tilde{\chi}_2^0 \tilde{\chi}_1^\pm$ and $\tilde{\chi}_2^0 \tilde{\chi}_1^0$. The masses of the neutralinos ($\tilde{\chi}_{1,2}^0$) were varied while the chargino mass was set to $\tilde{\chi}_1^\pm = \frac{1}{2}\left[m(\tilde{\chi}_1^0) + m(\tilde{\chi}_2^0)\right]$. Mass splittings in the case of pure Higgsinos are generated by radiative corrections, and are of the order of hundreds of MeV [47]. Mass splittings of the order of tens of GeV can be obtained by introducing mixing with wino or bino states. In this simplified model, mass differences ranging from 1 GeV to 60 GeV are considered, but the calculated cross sections assumed electroweakino mixing matrices corresponding to pure Higgsino $\widetilde{\chi}_2^0$, $\widetilde{\chi}_1^\pm$ and $\widetilde{\chi}_1^0$ states, and all other SUSY particles are decoupled. Example values of cross sections for $m(\widetilde{\chi}_2^0) = 110$ GeV and $m(\widetilde{\chi}_1^0) = 100$ GeV are 4.3 ± 0.1 pb for $\widetilde{\chi}_2^0 \widetilde{\chi}_1^\pm$ production and 2.73 ± 0.07 pb for $\widetilde{\chi}_2^0 \widetilde{\chi}_1^0$ production. The samples were generated at leading order (LO) with MG5_aMC@NLO 2.6.1 using the NNPDF23LO [48] parton distribution function (PDF) set and included up to two extra partons in the matrix element (ME). The electroweakinos were decayed with

[2] ATLAS uses a right-handed coordinate system with its origin at the nominal interaction point (IP) in the center of the detector and the z-axis along the beam pipe. The x-axis points from the IP to the center of the LHC ring, and the y-axis points upwards. Cylindrical coordinates (r, ϕ) are used in the transverse plane, ϕ being the azimuthal angle around the z-axis. The pseudorapidity is defined in terms of the polar angle θ as $\eta = -\ln\tan(\theta/2)$. Angular distance is measured in units of $\Delta R \equiv \sqrt{(\Delta\eta)^2 + (\Delta\phi)^2}$. Rapidity is defined by $y = \frac{1}{2}\ln[(E + p_z)/(E - p_z)]$, where E is the energy and p_z is the longitudinal component of the momentum along the beam direction.

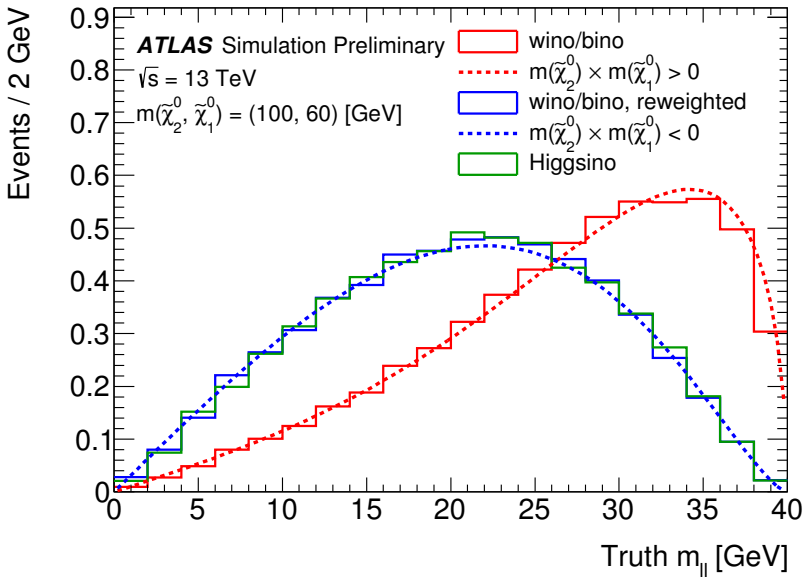

Figure 2: Dilepton invariant mass for Higgsino and wino/bino simplified models. The endpoint of the distribution is determined by the difference between the masses of the $\tilde{\chi}_2^0$ and $\tilde{\chi}_1^0$. The results from simulation (histograms) are compared against analytic calculations of the expected lineshape (dashed lines) presented in Ref. [53]. The product of the signed mass eigenvalues $\left(m\left(\tilde{\chi}_2^0\right) \times m\left(\tilde{\chi}_1^0\right)\right)$ is negative for Higgsino and can be either negative or positive for wino/bino scenarios.

with MadSpin [49]. The events were then interfaced with Pythia 8.212 [50] to model the parton shower (PS), hadronisation, and underlying event (UE) using the A14 set of tuned parameters (tune) [51]. The ME-PS matching was performed using the CKKW-L scheme [52] with the merging scale set to 15 GeV. To enforce an ISR topology, at least one parton in the final state is required to have a transverse momentum (p_{T}) greater than 50 GeV. Possible diagrams including coloured SUSY particles were excluded from the generation.

In the wino/bino scenario, the generated process is $pp \rightarrow \tilde{\chi}_2^0\tilde{\chi}_1^{\pm}$. The $\tilde{\chi}_1^0$ is a pure bino state, with the $\tilde{\chi}_2^0$ and $\tilde{\chi}_1^{\pm}$ states forming degenerate pure wino states. The generator configurations as well as the electroweakino decay branching ratios are consistent with those for the Higgsino samples. An example value of $\tilde{\chi}_2^0\tilde{\chi}_1^{\pm}$ production cross-section for $m(\tilde{\chi}_2^0) = m(\tilde{\chi}_1^{\pm}) = 110$ GeV is 16.0 ± 0.5 pb.

The electroweakino searches exploit the kinematic endpoint in the dilepton invariant mass spectrum from the decay chain $\tilde{\chi}_2^0 \rightarrow Z^*\tilde{\chi}_1^0$, $Z^* \rightarrow \ell\ell$. Therefore, processes that involve the production of a $\tilde{\chi}_2^0$ neutralino dominate the sensitivity of the search. The branching ratios for the processes $\tilde{\chi}_2^0 \rightarrow Z^*\tilde{\chi}_1^0$ and $\tilde{\chi}_1^{\pm} \rightarrow W^{\pm *}\tilde{\chi}_1^0$ were fixed to 100% for all above scenarios. The branching ratios of $Z^* \rightarrow \ell\ell$ and $W^{\pm *} \rightarrow \ell\nu$ depend on the invariant mass of the off-shell vector boson. For consistency with previous searches in the wino/bino scenario, the $Z^* \rightarrow \ell\ell$ branching ratios were set to a constant value corresponding to the on-shell Z branching ratios. For the Higgsino simplified model, the branching ratios were computed with SUSY-HIT 1.5a [54] which accounts for finite b-quark and τ masses. At $\Delta m\left(\tilde{\chi}_2^0, \tilde{\chi}_1^0\right) = 40$ GeV the $Z^* \rightarrow \ell\ell$ branching ratio for electrons or muons is 3.5%. This increases to 5.3% and 5.0% respectively at $\Delta m\left(\tilde{\chi}_2^0, \tilde{\chi}_1^0\right) = 1$ GeV due to the kinematic inaccessibility of heavier quarks and τ leptons. Similarly for $W^* \rightarrow \ell\nu$ the branching ratios to electrons or muons are both 11% at a mass splitting of 40 GeV, which increases to 20% and 17% respectively with $\Delta m\left(\tilde{\chi}_2^0, \tilde{\chi}_1^0\right) = 1$ GeV. The lineshape of the dilepton invariant

mass from the decay of the virtual Z^* depends on the relative sign of the $\widetilde{\chi}_1^0$ and $\widetilde{\chi}_2^0$ mass parameters. In the pure Higgsino case the product of the signed mass eigenvalues $\left(m\left(\tilde{\chi}_2^0\right) \times m\left(\tilde{\chi}_1^0\right)\right)$ is negative, while for the wino/bino case either $m\left(\tilde{\chi}_2^0\right) \times m\left(\tilde{\chi}_1^0\right) < 0$ or $m\left(\tilde{\chi}_2^0\right) \times m\left(\tilde{\chi}_1^0\right) > 0$ can occur. The generated wino/bino process assumes the product of the signed mass eigenstates is positive and the analytical description of the expected lineshape is used to reweight the $m_{\ell\ell}$ distribution to the negative product assumption. The difference between wino/bino and Higgsino lineshapes, as well as the reweighted distribution's agreement with the expected lineshape is shown in Figure 2.

For the third scenario, samples with direct production of selectrons $\tilde{e}_{L,R}$ or smuons $\tilde{\mu}_{L,R}$ are generated. The L, R subscripts denote left- or right-handed chirality of the sleptons. All sleptons flavours and chirality contributions are assumed to be degenerate in mass. An example value of the slepton production cross-section for $m(\widetilde{\ell}_{L,R}) = 110$ GeV is 0.55 ± 0.01 pb. These particles are decayed with a 100% branching ratio to their corresponding SM partner lepton and a pure bino neutralino, $\tilde{\chi}_1^0$. The slepton samples were generated with MG5_aMC@NLO 2.6.1 and interfaced with Pythia 8.230. The PDF set used was NNPDF2.3LO with the A14 tune. Similar to the the Higgsino and wino/bino samples, CKKW-L merging was used for the ME-PS matching [55], with the merging scale set to a quarter of the sleptons' mass.

Cross sections for the signal scenarios are calculated with Resummino 2.0.1 [56–58] at NLL+NLO precision. The evaluation of the cross section and corresponding uncertainty are taken from an envelope of cross section predictions using different PDF sets, and varied factorisation and normalisation scales. This procedure is described in more detail in Ref. [59], and is the same procedure used in the previous search result [41].

The SM processes are estimated from a combination of Monte Carlo (MC) simulation as well as data-driven approaches. The latter are described in Section 6. Sherpa 2.2.1 and 2.2.2 [60] were used to model the V+jets ($V = W, Z, \gamma^*$) samples involving leptonically decaying vector bosons, as well as diboson (WW, ZZ and WZ, collectively referred to as VV), and fully leptonic triboson processes. Vector boson fusion (VBF) and gluon-gluon fusion (ggF) single higgs production were generated with Powheg-Box [61], while higgs production in association with a massive vector boson was generated with Pythia 8.186, and ttH production was generated with MG5_aMC@NLO 2.2.3. Single top, $t\bar{t}$, and top quarks produced in association with W bosons were all generated with Powheg-Box. Rarer top processes all used MG5_aMC@NLO (versions 2.2.2/2.3.3). ME processes, excluding those generated with Pythia or Sherpa, were then interfaced with Pythia 8 using the ME+PS prescription. Further details on the configuration of the SM processes can be found in Refs. [62–66]. A summary of the generator configurations, including the PDF sets and cross sections used for normalisation is found in Table 1.

To simulate the effects of additional pp collisions, referred to as pileup, in the same and neighbouring bunch crossings, additional interactions were generated using the soft QCD processes of Pythia 8.186 with the A3 tune [81] and the MSTW2008LO PDF set [82], and were overlaid onto each simulated hard-scatter event. The MC samples were reweighted to match the pileup distribution observed in the data.

All MC simulated samples were processed through the ATLAS simulation framework [83] in Geant4 [84]. The samples for the signal scenarios made use of the ATLAS fast simulation, which parameterises the response of the calorimeters. Background and signal samples made use of EvtGev 1.6.0 and 1.2.0 [85] to model the decay of bottom and charm quarks, with exception to background samples modelled with Sherpa.

Process	Matrix element	Parton shower	PDF set	Cross section
V+jets	Sherpa 2.2.1		NNPDF 3.0 NNLO [67]	NNLO [68]
VV	Sherpa 2.2.1/2.2.2		NNPDF 3.0 NNLO	Generator NLO
Triboson	Sherpa 2.2.1		NNPDF 3.0 NNLO	Generator LO, NLO
$h[ggF]$	Powheg-Box	Pythia 8.212	NLO CTEQ6L1 [69]	N^{3}LO [70]
$h[VBF]$	Powheg-Box	Pythia 8.186	NLO CTEQ6L1 [69]	NNLO + NLO [70]
$h + W/Z$	Pythia 8.186		NNPDF 2.3 LO [48]	NNLO + NLO [70]
$h + t\bar{t}$	MG5_aMC@NLO 2.2.3	Pythia 8.210	NNPDF 2.3 LO	NLO [70]
$t\bar{t}$	Powheg-Box	Pythia 8.230	NNPDF 2.3 LO	NNLO+NNLL [71–75]
t (s-channel)	Powheg-Box	Pythia 8.230	NNPDF 2.3 LO	NNLO+NNLL [76]
t (t-channel)	Powheg-Box	Pythia 8.230	NNPDF 2.3 LO	NNLO+NNLL [77, 78]
$t + W$	Powheg-Box	Pythia 8.230	NNPDF 2.3 LO	NNLO+NNLL [79]
$t + Z$	MG5_aMC@NLO 2.3.3	Pythia 8.212	NNPDF 2.3 LO	NLO [80]
$t\bar{t}WW$	MG5_aMC@NLO 2.2.2	Pythia 8.186	NNPDF 2.3 LO	NLO [80]
$t\bar{t} + Z/W/\gamma^*$	MG5_aMC@NLO 2.3.3	Pythia 8.210/8.212	NNPDF 2.3 LO	NLO [70]
$t + WZ$	MG5_aMC@NLO 2.3.3	Pythia 8.212	NNPDF 2.3 LO	NLO [80]
$t + t\bar{t}$	MG5_aMC@NLO 2.2.2	Pythia 8.186	NNPDF 2.3 LO	LO [80]
$tt\bar{t}\bar{t}$	MG5_aMC@NLO 2.2.2	Pythia 8.186	NNPDF 2.3 LO	NLO [80]

Table 1: Simulated SM background processes. The PDF set refers to that used in for the matrix element.

4 Event Reconstruction

Candidate events are required to have at least one reconstructed pp interaction vertex with a minimum of two associated tracks with $p_{\mathrm{T}} > 500$ MeV. In events with multiple vertices, the primary vertex is defined as the one with the highest $\sum p_{\mathrm{T}}^2$ of associated tracks. To reject events with detector noise or non-collision backgrounds, a set of basic quality criteria [86] are applied.

Leptons, jets and tracks are "preselected" using loose identification criteria, and must survive tighter "signal" identification requirements in order to be selected for the search regions. Preselected leptons and jets are used in fake/nonprompt (FNP) background estimates as well as in resolving ambiguities between tracks and clusters associated with multiple lepton and jet candidates.

Isolation criteria are used in the definition of signal leptons, and are based on tracking information, calorimeter clusters, or both. Isolation energies are computed as a $\sum p_{\mathrm{T}}$ of nearby activity, excluding the contributions from nearby leptons, and are effective in reducing contributions from semileptonic heavy-flavour hadron decays and jets faking prompt leptons. The isolation requirements used in this analysis are based on those described in Refs. [87] and [88], with updates to improve their performance under the increased pileup conditions encountered in the 2017 and 2018 data samples.

Electrons are required to have $p_{\mathrm{T}} > 4.5$ GeV and $|\eta| < 2.47$. Preselected electrons are further required to pass the calorimeter- and tracking-based *VeryLoose* likelihood identification [88], and to have a longitudinal impact parameter z_0 relative to the primary vertex that satisfies $|z_0 \sin\theta| < 0.5$ mm. Signal electrons must satisfy the *Medium* identification criterion [88], and be compatible with originating from the primary vertex, with the significance of the transverse impact parameter defined relative to the beam position satisfying $|d_0|/\sigma(d_0) < 5$. Signal electrons are further refined using the *Gradient* isolation working point [88], which uses both tracking and calorimeter information.

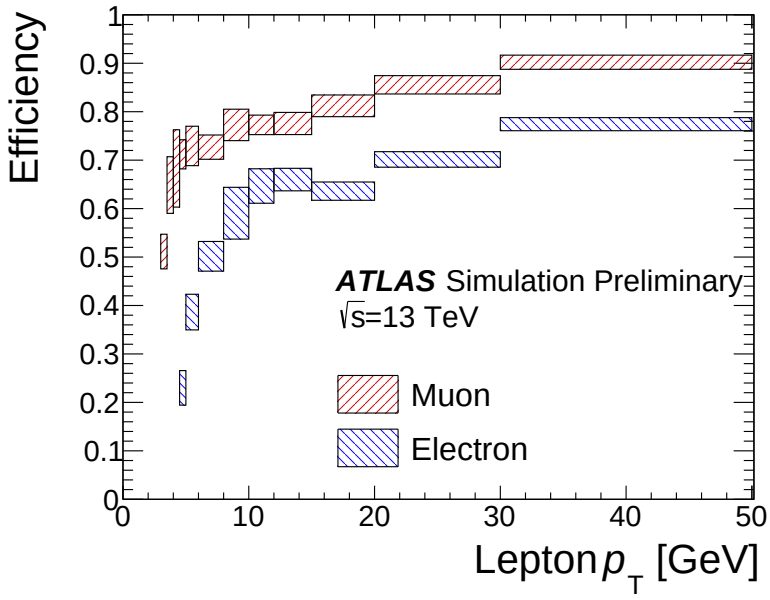

Figure 3: Signal lepton efficiencies for electrons and muons in a mix of slepton and Higgsino samples. Combined reconstruction, identification, isolation and vertex association efficiencies are shown for leptons within detector acceptance, and with lepton p_{T} within a factor of 3 of $\Delta m(\widetilde{\ell}, \widetilde{\chi}_1^0)$ for sleptons or of $\Delta m(\widetilde{\ell}, \widetilde{\chi}_1^0)/2$ for Higgsinos. The average number of interactions per crossing in the MC samples is $\langle\mu\rangle = 33.7$. Uncertainty bands represent the range of efficiencies observed across all signal samples used for the given p_{T} bin. The η-dependence is consistent with values reported in ATLAS combined performance papers.

Muons are required to satisfy $p_{\mathrm{T}} > 3$ GeV and $|\eta| < 2.5$. Preselected muons are identified using the *LowPt* criterion, a re-optimised selection similar to those defined in Ref. [87] but with improved signal efficiency and background rejection for $p_{\mathrm{T}} < 10$ GeV muon candidates. Preselected muons must also satisfy $|z_0 \sin\theta| < 0.5$ mm. From the remaining preselected muons, signal muons must satisfy $|d_0|/\sigma(d_0) < 3$. Finally, signal muons are required to pass the *FCTightTrackOnly* isolation working point, which uses only tracking information.

After all lepton selection criteria are applied, the efficiency for reconstructing and identifying signal electrons within the detector acceptance in the Higgsino and slepton signal samples ranges from 20% for $p_{\mathrm{T}} = 4.5$ GeV to over 75% for $p_{\mathrm{T}} > 30$ GeV. The corresponding efficiency for signal muons ranges from approximately 50% at $p_{\mathrm{T}} = 3$ GeV to 90% for $p_{\mathrm{T}} > 30$ GeV. The efficiency for signal electrons and muons in a mix of slepton and Higgsino samples is shown in Fig. 3 as a function of lepton p_{T}.

Preselected jets are reconstructed from calorimeter topological energy clusters [89] in the region $|\eta| < 4.5$ using the anti-k_t algorithm [90, 91] with radius parameter $R = 0.4$. The jets are required to have $p_{\mathrm{T}} > 20$ GeV after being calibrated in accord with Ref. [92] and having the expected energy contribution from pileup subtracted according to the jet area [93]. In order to suppress jets due to pileup, jets with $p_{\mathrm{T}} < 120$ GeV and $|\eta| < 2.5$ are required to satisfy the *Medium* working point of the jet vertex tagger [93], which uses information from the tracks associated to the jet. From the sample of preselected jets, signal jets are selected if they satisfy $p_{\mathrm{T}} > 30$ GeV and $|\eta| < 2.8$.

Jets identified as containing b-hadron decays, referred to as b-tagged jets, are identified from preselected jets within $|\eta| < 2.5$ using the *MV2c10* algorithm [94, 95]. The $p_{\mathrm{T}} > 20$ GeV requirement is maintained to maximise the rejection of the $t\bar{t}$ background. The b-tagging algorithm working point is chosen so that b-jets

from simulated $t\bar{t}$ events are identified with an 85% efficiency, with rejection factors of 3 for charm-quark jets and 34 for light-quark and gluon jets.

The following procedure is used to resolve ambiguities between the reconstructed leptons and jets. It employs the distance measure $\Delta R_y = \sqrt{(\Delta y)^2 + (\Delta\phi)^2}$, where y is the rapidity. Electrons that share an inner detector track with a muon candidate are discarded to remove bremsstrahlung from muons followed by a photon conversion. Non-b-tagged jets that are separated from the remaining electrons by $\Delta R_y < 0.2$ are removed. Jets containing a muon candidate within $\Delta R_y < 0.4$ and with fewer than three tracks with $p_{\mathrm{T}} > 500$ MeV are removed to suppress muon bremsstrahlung. Electrons or muons with $\Delta R_y < 0.4$ from surviving jet candidates are removed to suppress bottom and charm hadron decays.

In order to increase the efficiency for signals with the lowest mass splittings, where the lepton p_{T} can be very low, signal regions based on a signal lepton and an isolated low-p_{T} track are used. For these regions the track is selected to be matched to a reconstructed electron or muon candidate with no identification requirements. Preselected tracks with $p_{\mathrm{T}} > 500$ MeV and $\eta < 2.5$ are selected using the *Tight-Primary* working point defined in Ref. [96]. Signal tracks are required to be within $\Delta R < 0.01$ of a reconstructed electron or muon candidate. Electron (muon) candidates can be reconstructed with transverse momenta as low as 1 (2) GeV, and are required to fail the signal requirements defined above to avoid any overlap. Signal tracks with p_{T} that differs from the transverse momentum of the matched lepton by more than 20% are rejected. The track-lepton matching allows for the tracks to be identified as electron or muon tracks, reducing backgrounds from tracks not originating from the leptonic decay of a SUSY particle. Signal tracks must also satisfy dedicated isolation criteria – they are required to be separated from preselected jets by at least $\Delta R > 0.5$, and the $\sum p_{\mathrm{T}}$ of preselected tracks within $\Delta R < 0.3$ of signal tracks, excluding the contributions from nearby leptons, is required to be smaller than 0.5 GeV. Finally, signal tracks must satisfy $p_{\mathrm{T}} > 1$ GeV, $|z_0 \sin\theta| < 0.5$ mm and $|d_0|/\sigma(d_0) < 3$. The efficiency of selecting signal tracks for the studied electroweakino signals is 20% for electrons with $3 < p_{\mathrm{T}} < 4$ GeV and 35% for muons with $2 < p_{\mathrm{T}} < 3$ GeV.

Small corrections are applied to reconstructed electrons, muons, b-tagged jets, and tracks in the simulated samples to match the reconstruction efficiencies in data. The corrections for b-tagged jets account for the differences between data and simulated samples in the identification efficiencies for jets including b-hadron decays, as well as mis-identification rates of c-, and light-flavour / gluon initiated jets. The corrections for low-momentum leptons are obtained from $J/\psi \to ee/\mu\mu$ events with the same tag-and-probe methods as used for higher-p_{T} electrons [88] and muons [87]. The corrections used to account for track-lepton matching efficiency differences in data and simulation are derived with J/ψ events decaying to a low-p_{T} signal lepton and a preselected track. The track isolation corrections are measured using Z events decaying to a signal lepton and a track matched to a reconstructed lepton candidate. All track corrections are found to be compatible with 1. Dedicated scale factors are also applied in MC to properly model the trigger efficiency observed in data. These scale factor are measured in events selected with single muon triggers, passing kinematic selections similar to the ones used to define the SRs. They are parametrised as a function of $E_{\mathrm{T}}^{\mathrm{miss}}$ and found to vary between 0.9 and 1 in the $E_{\mathrm{T}}^{\mathrm{miss}}$ range of interest. An uncertainty of 5% is assigned to the scale factors to cover their dependence with other kinematic quantities.

The missing transverse momentum $\mathbf{p}_{\mathrm{T}}^{\mathrm{miss}}$, with magnitude $E_{\mathrm{T}}^{\mathrm{miss}}$, is defined as the negative vector sum of the transverse momenta of all reconstructed objects (electrons, muons, jets, and photons [97]) and an additional soft term. A dedicated overlap removal procedure is used to resolve ambiguities between the reconstructed objects [98]. The soft term is constructed from all tracks that are not associated with any lepton or jet, but that are associated with the primary vertex. In this way, $E_{\mathrm{T}}^{\mathrm{miss}}$ is adjusted for the best calibration of jets and leptons, while maintaining pileup independence in the soft term [98].

	Preselection requirements	
Variable	2ℓ	$1\ell 1T$
Number of leptons (tracks)	= 2 leptons	= 1 lepton and ≥ 1 track
Lepton p_{T} [GeV]	$p_{\mathrm{T}}^{\ell_1} > 5$	$p_{\mathrm{T}}^{\ell} < 10$
$\Delta R_{\ell\ell}$	$\Delta R_{ee} > 0.30$, $\Delta R_{\mu\mu} > 0.05$, $\Delta R_{e\mu} > 0.2$	$0.05 < \Delta R_{\ell\mathrm{track}} < 1.5$
Lepton (track) charge and flavor	$e^{\pm}e^{\mp}$ or $\mu^{\pm}\mu^{\mp}$	$e^{\pm}e^{\mp}$ or $\mu^{\pm}\mu^{\mp}$
Lepton (track) invariant mass [GeV]	$3 < m_{ee} < 60$, $1 < m_{\mu\mu} < 60$	$0.5 < m_{\ell\mathrm{track}} < 5$
J/ψ invariant mass [GeV]	veto $3 < m_{\ell\ell} < 3.2$	veto $3 < m_{\ell\mathrm{track}} < 3.2$
$m_{\tau\tau}$ [GeV]	< 0 or > 160	no requirement
$E_{\mathrm{T}}^{\mathrm{miss}}$ [GeV]	> 120	> 120
Number of jets	≥ 1	≥ 1
Number of b-tagged jets	= 0	no requirement
Leading jet p_{T} [GeV]	≥ 100	≥ 100
$\min(\Delta\phi(\text{any jet}, \mathbf{p}_{\mathrm{T}}^{\mathrm{miss}}))$	> 0.4	> 0.4
$\Delta\phi(j_1, \mathbf{p}_{\mathrm{T}}^{\mathrm{miss}})$	≥ 2.0	≥ 2.0

Table 2: Preselection requirements applied to all events entering into electroweakino and slepton search regions.

5 Signal Regions

Events entering into all SRs share a common preselection, with requirements listed in Table 2. The $1\ell 1T$ channel requires exactly one signal lepton and at least one signal track of the same flavour and opposite electric charge (OS); all other regions require exactly two OS signal leptons, also of the same flavour. In regions with two leptons, the higher-p_{T} lepton is denoted the "leading" lepton (ℓ_1) while the lower-p_{T} lepton is the "subleading" lepton (ℓ_2).

Preselection requirements are employed to reduce backgrounds and form a basis for SRs and CRs used in the simultaneous fit. The leading lepton is required to have $p_{\mathrm{T}} > 5$ GeV, which reduces backgrounds from FNP leptons. Pairs of electrons are required to be separated by $\Delta R_{ee} > 0.3$ to avoid reconstruction inefficiencies due to overlapping electron showers in the EM calorimeter, while electrons and muons are likewise required to be separated by $\Delta R_{e\mu} > 0.2$ to avoid energy deposits from muons spoiling electron shower shapes. An additional requirement that $m_{\ell\ell}$ be outside of $[3.0, 3.2]$ GeV removes contributions from J/ψ decays, while requiring $m_{\ell\ell} < 60$ GeV reduces contributions from on-shell Z-boson decays. Contributions from other hadronic resonances, e.g. Υ states, are expected to be negligible in the search regions and are not explicitly vetoed. Requirements on the minimal angular separation between the lepton candidates ($\Delta R_{\ell\ell}$) and invariant mass ($m_{\ell\ell}$) removes events in which an energetic photon produces collinear lepton pairs.

The $m_{\tau\tau}$ variable [99–101] is defined as $m_{\tau\tau} = \mathrm{sign}\left(m_{\tau\tau}^2\right)\sqrt{\left|m_{\tau\tau}^2\right|}$, which is the signed square root of $m_{\tau\tau}^2 \equiv 2p_{\ell_1} \cdot p_{\ell_2}(1+\xi_1)(1+\xi_2)$, where p_{ℓ_1} and p_{ℓ_2} are the lepton four-momenta, while the parameters ξ_1 and ξ_2 are determined by solving $\mathbf{p}_{\mathrm{T}}^{\mathrm{miss}} = \xi_1\mathbf{p}_{\mathrm{T}}^{\ell_1} + \xi_2\mathbf{p}_{\mathrm{T}}^{\ell_2}$. The definition of $m_{\tau\tau}$ approximates the invariant mass of a leptonically decaying τ-lepton pair if both τ-leptons are sufficiently boosted so that the neutrinos from each τ decay are collinear with the visible lepton momentum. The $m_{\tau\tau}$ variable can be less than zero in events where one of the lepton momenta has a smaller magnitude than the $E_{\mathrm{T}}^{\mathrm{miss}}$ and points in the hemisphere opposite to the $\mathbf{p}_{\mathrm{T}}^{\mathrm{miss}}$ vector. Events with $0 < m_{\tau\tau} < 160$ GeV are rejected, a requirement that reduces backgrounds from $Z \to \tau\tau$ and has an efficiency greater than 80% for the signals considered.

	Electroweakino SR Requirements			
Variable	Low-$E_{\mathrm{T}}^{\mathrm{miss}}$, low-$\Delta m$	Low-$E_{\mathrm{T}}^{\mathrm{miss}}$, high-$\Delta m$	High-$E_{\mathrm{T}}^{\mathrm{miss}}$	$1\ell 1T$
$E_{\mathrm{T}}^{\mathrm{miss}}$ [GeV]	[120, 200]	[120, 200]	> 200	> 200
$E_{\mathrm{T}}^{\mathrm{miss}}/H_{\mathrm{T}}^{\mathrm{lep}}$	> 10	< 10	–	> 30
$\Delta\phi(\mathrm{lep}, \mathbf{p}_{\mathrm{T}}^{\mathrm{miss}})$	–	–	–	< 1.0
Lepton or track p_{T} [GeV]	–	$p_{\mathrm{T}}^{\ell_2} > 5 + m_{\ell\ell}/4$	$p_{\mathrm{T}}^{\ell_2} > \min(10, 2 + m_{\ell\ell}/3)$	$p_{\mathrm{T}}^{\mathrm{track}} < 5$
$M_{\mathrm{T}}^{\mathrm{S}}$ [GeV]	< 50	–	–	–
$m_{\mathrm{T}}^{\ell_1}$ [GeV]	–	[10, 60]	< 60	–
R_{ISR}	–	[0.8, 1.0]	$[\max(0.85, 0.98 - 0.02 \times m_{\ell\ell}),\ 1.0]$	–

Table 3: Requirements applied to all events entering into signal regions used for electroweakino searches.

The reconstructed $E_{\mathrm{T}}^{\mathrm{miss}}$ is required to be greater than 120 GeV in preselection, with higher thresholds applied to different SRs. For SUSY events in which much of the invisible momentum is carried by the $\widetilde{\chi}_1^0$ pair, these requirements on $E_{\mathrm{T}}^{\mathrm{miss}}$ suggest that the SUSY system is recoiling against additional hadronic activity in the form of an ISR jet. All events are therefore required to have at least one jet with $p_{\mathrm{T}} > 100$ GeV, with that jet being separated from the $\mathbf{p}_{\mathrm{T}}^{\mathrm{miss}}$ by at least 2.0 radians in ϕ. Additional jets in the event are also required to be separated from the $\mathbf{p}_{\mathrm{T}}^{\mathrm{miss}}$ by $\min(\Delta\phi(\text{any jet}, \mathbf{p}_{\mathrm{T}}^{\mathrm{miss}}))>0.4$ in order to suppress the impact of jet energy mismeasurement on $E_{\mathrm{T}}^{\mathrm{miss}}$. Events with one or more b-tagged jets with $p_{\mathrm{T}} > 20$ GeV ($N_{b-\mathrm{jet}}^{20}$) are vetoed to reduce backgrounds from $t\bar{t}$ production.

After applying the preselection requirements above, SRs are further optimised for specific SUSY scenarios. Two categories of SRs are constructed: one for electroweakinos and the other targeting sleptons.

The SRs designed for sensitivity to electroweakinos are defined in Table 3. High-$E_{\mathrm{T}}^{\mathrm{miss}}$ regions require $E_{\mathrm{T}}^{\mathrm{miss}} > 200$ GeV, where the online $E_{\mathrm{T}}^{\mathrm{miss}}$ triggers are fully efficient for the SUSY signal. Two Low-$E_{\mathrm{T}}^{\mathrm{miss}}$ regions are constructed using events with 120 GeV $< E_{\mathrm{T}}^{\mathrm{miss}} <$ 200 GeV: one targeting electroweakinos with small mass splittings (Low-$E_{\mathrm{T}}^{\mathrm{miss}}$, low-$\Delta m$), and one targeting mass splittings larger than $\sim$ 10 GeV (Low-$E_{\mathrm{T}}^{\mathrm{miss}}$, high-$\Delta m$).

The p_{T} threshold for the subleading lepton is defined with sliding cuts that retain efficiency for soft leptons from low-Δm signals while reducing backgrounds from FNP leptons in events with larger values of $m_{\ell\ell}$. The sliding requirement was optimised using a Z_N significance metric [102] separately in each SR, considering signal models with a variety of masses and mass splittings.

The transverse mass of the leading lepton and $E_{\mathrm{T}}^{\mathrm{miss}}$ is defined as $m_{\mathrm{T}}^{\ell_1} = \sqrt{2(E_{\mathrm{T}}^{\ell_1} E_{\mathrm{T}}^{\mathrm{miss}} - \mathbf{p}_{\mathrm{T}}^{\ell_1} \cdot \mathbf{p}_{\mathrm{T}}^{\mathrm{miss}})}$ and is used in the Low-$E_{\mathrm{T}}^{\mathrm{miss}}$, high-$\Delta m$ and High-$E_{\mathrm{T}}^{\mathrm{miss}}$ regions to reduce contributions from fake and nonprompt leptons.

In events with high-p_{T} ISR jets, the axis of maximum back-to-back p_{T}, referred to here as the thrust axis, approximates the direction of the recoil between the ISR activity and the sparticle pair. The recursive jigsaw reconstruction (RJR) technique [42] is used to divide each event into two hemispheres perpendicular to the thrust axis: a supersymmetric particles hemisphere S, expected to contain the decay products of the electroweakinos or slepton pair and therefore the $E_{\mathrm{T}}^{\mathrm{miss}}$; and an ISR hemisphere, containing hadronic activity. This bisection allows the calculation of two discriminating variables that are useful in isolating events with ISR-induced $E_{\mathrm{T}}^{\mathrm{miss}}$ topologies: R_{ISR}, the ratio between the $E_{\mathrm{T}}^{\mathrm{miss}}$ and the transverse momentum of the ISR system, and $M_{\mathrm{T}}^{\mathrm{S}}$, the transverse mass of the S system. The R_{ISR} variable in particular is sensitive to the mass splitting, with values near 1.0 for the most compressed SUSY events. Figure 4 shows the

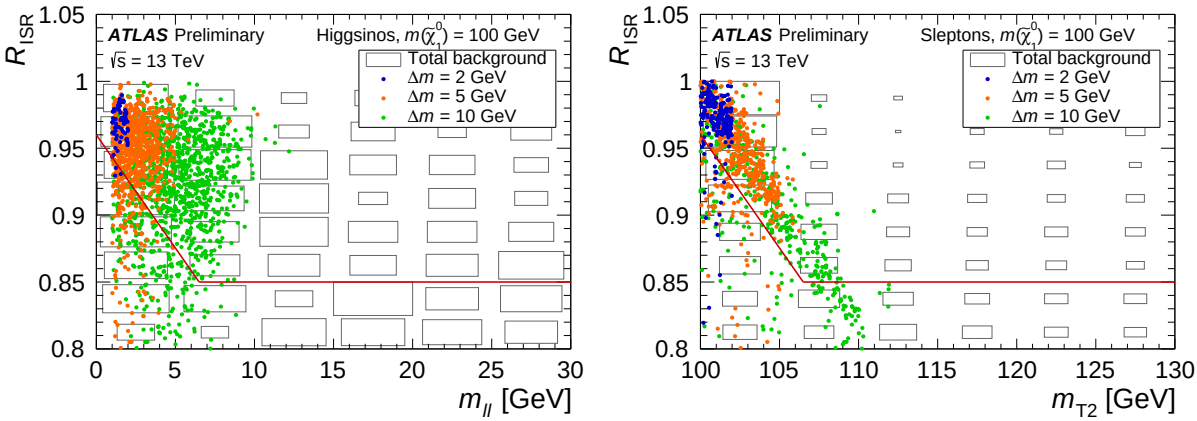

Figure 4: Distributions of R_{ISR} for the electroweakino (left) and slepton (right) High-$E_{\mathrm{T}}^{\mathrm{miss}}$ SRs, after applying all signal selection criteria except those on R_{ISR}. The solid red line indicates the requirement applied in the signal region; events in the region below the red line are rejected. Representative benchmark signals for the Higgsino (left) and slepton (right) simplified models are shown as circles.

relationship between R_{ISR} and $m_{\ell\ell}$ and m_{T2}, which is exploited in the High-$E_{\mathrm{T}}^{\mathrm{miss}}$ SRs through sliding requirements on R_{ISR}.

The $E_{\mathrm{T}}^{\mathrm{miss}}/H_{\mathrm{T}}^{\mathrm{lep}}$ variable, where $H_{\mathrm{T}}^{\mathrm{lep}}$ is the scalar sum of the p_{T} of the two leptons, has been shown to be an effective discriminant for SUSY signals [41]. In these SRs, the Low-$E_{\mathrm{T}}^{\mathrm{miss}}$ regions are made orthogonal by requiring $E_{\mathrm{T}}^{\mathrm{miss}}/H_{\mathrm{T}}^{\mathrm{lep}} > 10$ for Low-$E_{\mathrm{T}}^{\mathrm{miss}}$, low-$\Delta m$, where $H_{\mathrm{T}}^{\mathrm{lep}}$ is typically smaller for the SUSY signal, and $E_{\mathrm{T}}^{\mathrm{miss}}/H_{\mathrm{T}}^{\mathrm{lep}} < 10$ for Low-$E_{\mathrm{T}}^{\mathrm{miss}}$, high-$\Delta m$, where $H_{\mathrm{T}}^{\mathrm{lep}}$ increases due to the larger mass splitting.

The $1\ell 1T$ channel targets SUSY signals with especially low values of Δm, which produce very low-momentum decay products. This channel therefore requires that the identified lepton has $p_{\mathrm{T}} < 10$ GeV and that the track has $p_{\mathrm{T}} < 5$ GeV. The lepton is also required to be within 1.0 radians of the $\mathbf{p}_{\mathrm{T}}^{\mathrm{miss}}$ in ϕ, to reduce backgrounds with tracks associated to non-prompt leptons or hadrons. Finally, the $1\ell 1T$ channel requires $E_{\mathrm{T}}^{\mathrm{miss}}/H_{\mathrm{T}}^{\mathrm{lep}} > 10$, where in this case $H_{\mathrm{T}}^{\mathrm{lep}}$ is the scalar sum of lepton and track p_{T}, again exploiting the low values of $H_{\mathrm{T}}^{\mathrm{lep}}$ expected for signal models with small mass splittings.

The SRs designed to give sensitivity for slepton production are defined in Table 4. The slepton search exploits the relationship between the mass splitting and the lepton and $E_{\mathrm{T}}^{\mathrm{miss}}$ kinematics via the stransverse mass (m_{T2}) variable [25, 26]. The stransverse mass is defined as:

$$m_{\mathrm{T2}}^{m_\chi}\left(\mathbf{p}_{\mathrm{T}}^{\ell_1}, \mathbf{p}_{\mathrm{T}}^{\ell_2}, \mathbf{p}_{\mathrm{T}}^{\mathrm{miss}}\right) = \min_{\mathbf{q}_{\mathrm{T}}}\left(\max\left[m_{\mathrm{T}}\left(\mathbf{p}_{\mathrm{T}}^{\ell_1}, \mathbf{q}_{\mathrm{T}}, m_\chi\right), m_{\mathrm{T}}\left(\mathbf{p}_{\mathrm{T}}^{\ell_2}, \mathbf{p}_{\mathrm{T}}^{\mathrm{miss}} - \mathbf{q}_{\mathrm{T}}, m_\chi\right)\right]\right),$$

where m_χ is the hypothesised mass of the invisible particles, and the transverse vector $\mathbf{q}_{\mathrm{T}}$ with magnitude q_{T} is chosen to minimise the larger of the two transverse masses, defined by

$$m_{\mathrm{T}}\left(\mathbf{p}_{\mathrm{T}}, \mathbf{q}_{\mathrm{T}}, m_\chi\right) = \sqrt{m_\ell^2 + m_\chi^2 + 2\left(\sqrt{p_{\mathrm{T}}^2 + m_\ell^2}\sqrt{q_{\mathrm{T}}^2 + m_\chi^2} - \mathbf{p}_{\mathrm{T}} \cdot \mathbf{q}_{\mathrm{T}}\right)}.$$

For signal events with slepton mass $m(\widetilde{\ell})$ and LSP mass $m(\widetilde{\chi}_1^0)$, the values of $m_{\mathrm{T2}}^{m_\chi}$ are bound from above by $m(\widetilde{\ell})$ when m_χ is equal to $m(\widetilde{\chi}_1^0)$, i.e. $m_{\mathrm{T2}}^{m_\chi} \leq m(\widetilde{\ell})$ for $m_\chi = m(\widetilde{\chi}_1^0)$. The stransverse mass with

	Slepton SR Requirements	
Variable	Low-$E_{\mathrm{T}}^{\mathrm{miss}}$	High-$E_{\mathrm{T}}^{\mathrm{miss}}$
$E_{\mathrm{T}}^{\mathrm{miss}}$ [GeV]	$[150, 200]$	> 200
m_{T2} [GeV]	< 140	< 140
$p_{\mathrm{T}}^{\ell_2}$ [GeV]	$> \min(15, 7.5 + 0.75 \times (m_{\mathrm{T2}} - 100))$	$> \min(20, 2.5 + 2.5 \times (m_{\mathrm{T2}} - 100))$
R_{ISR}	$[0.8,\ 1.0]$	$[\max(0.85, 0.98 - 0.02 \times (m_{\mathrm{T2}} - 100)),\ 1.0]$

Table 4: Requirements applied to all events entering into signal regions used for slepton searches. The 2ℓ preselection requirements from Table 2 are implied.

$m_{\chi} = 100$ GeV, denoted m_{T2}^{100}, is used in this note. The chosen value of 100 GeV is based on the expected LSP masses of the signals targeted. The distribution of m_{T2}^{100} does not vary significantly for the signals considered where $m(\widetilde{\chi}_1^0) \neq 100$ GeV.

The Low-$E_{\mathrm{T}}^{\mathrm{miss}}$ slepton region uses events with 150 GeV $< E_{\mathrm{T}}^{\mathrm{miss}} <$ 200 GeV, while the High-$E_{\mathrm{T}}^{\mathrm{miss}}$ region uses events with $E_{\mathrm{T}}^{\mathrm{miss}} > 200$ GeV. The Low-$E_{\mathrm{T}}^{\mathrm{miss}}$ region contributes most significantly for signals with $\Delta m \gtrsim 10$ GeV, where the leptons satisfy the p_{T} thresholds without needing a significant additional boost from ISR jets. Both regions are constructed with sliding requirements on $p_{\mathrm{T}}^{\ell_2}$ following the strategy for the electroweakino regions above. The requirements on R_{ISR} are looser in the Low-$E_{\mathrm{T}}^{\mathrm{miss}}$ region, targeting less compressed scenarios, while the High-$E_{\mathrm{T}}^{\mathrm{miss}}$ region uses a sliding requirement on R_{ISR} to maintain sensitivity to the most compressed scenarios while reducing backgrounds for events with larger m_{T2}.

After all selection requirements are applied, the electroweakino SRs are binned in $m_{\ell\ell}$ and the slepton SRs are binned in m_{T2}. Electroweakino bin boundaries are at $m_{\ell\ell}$ =1, 2, 3, 5, 10, 20, 30, 40, and 60 GeV for the two lepton channels, and at 1, 1.5, 2, 2.5, 3, 4, and 5 GeV for the $1\ell 1T$ channel. The m_{T2} boundaries for the slepton searches are at 100.5, 101, 102, 105, 110, 120, 130, and 140 GeV. Events above $m_{\ell\ell} = 60$ GeV are rejected in preselection for all channels, and events above $m_{\mathrm{T2}} = 140$ GeV have minimal sensitivity to compressed sleptons and are not considered.

6 Background Estimation

The sources of SM background in regions with two leptons can be subdivided into two categories: reducible backgrounds from events where at least one of the candidate leptons is FNP, and irreducible backgrounds from events that contain two prompt leptons.

Since MC simulation is not expected to model processes with FNP leptons accurately, a data-driven method, referred to as the Fake Factor method [103], is employed to estimate these backgrounds. The yields obtained from this procedure are cross-checked in validation regions (VRs), named VR-SS.

The dominant sources of irreducible background are $t\bar{t}/tW$, WW/WZ, and $Z^{(*)}/\gamma^*(\rightarrow \tau\tau)$ + jets. These backgrounds are estimated using MC simulations normalised to data in dedicated CRs. Events originating from the production of Drell-Yan, triboson, Higgs boson and top quarks in association with gauge bosons constitute a small fraction of the total background. Their contributions in the regions with two leptons are estimated using the MC samples listed in Table 1. Additional VRs, referred to as VR-DF, are used to validate the extrapolation of background in the fitting procedure within the same kinematic regime as the SRs.

Region	SR orthogonality	Lepton Flavor	Additional requirements
CR-top-ewkino-high-$E_{\mathrm{T}}^{\mathrm{miss}}$ CR-top-ewkino-low-$E_{\mathrm{T}}^{\mathrm{miss}}$-high-$\Delta m$	$N_{b-\mathrm{jet}}^{20} \geq 1$	$ee + \mu\mu + e\mu + \mu e$	$R_{\mathrm{ISR}} \in [0.7, 1.0]$, $m_{\mathrm{T}}^{\ell_1}$ removed $E_{\mathrm{T}}^{\mathrm{miss}}/H_{\mathrm{T}}^{\mathrm{lep}}$ and $m_{\mathrm{T}}^{\ell_1}$ removed
CR-tau-ewkino-high-$E_{\mathrm{T}}^{\mathrm{miss}}$ CR-tau-ewkino-low-$E_{\mathrm{T}}^{\mathrm{miss}}$-high-$\Delta m$ VR-tau-ewkino-low-$E_{\mathrm{T}}^{\mathrm{miss}}$-low-$\Delta m$	$m_{\tau\tau} \in [60, 120]$ GeV	$ee + \mu\mu + e\mu + \mu e$	$R_{\mathrm{ISR}} \in [0.7, 1.0]$, $m_{\mathrm{T}}^{\ell_1}$ removed $R_{\mathrm{ISR}} \in [0.6, 1.0]$, $m_{\mathrm{T}}^{\ell_1}$ removed –
CR-VV-ewkino-high-$E_{\mathrm{T}}^{\mathrm{miss}}$ CR-VV-ewkino-low-$E_{\mathrm{T}}^{\mathrm{miss}}$-high-$\Delta m$	$R_{\mathrm{ISR}} \in [0.7, 0.85]$ $R_{\mathrm{ISR}} \in [0.6, 0.8]$	$ee + \mu\mu + e\mu + \mu e$	$m_{\mathrm{T}}^{\ell_1}$ removed $m_{\mathrm{T}}^{\ell_1} > 30$ GeV, $N_{\mathrm{jets}} = 1$, $E_{\mathrm{T}}^{\mathrm{miss}}/H_{\mathrm{T}}^{\mathrm{lep}}$ removed
VR-SS-ewkino-high-$E_{\mathrm{T}}^{\mathrm{miss}}$ VR-SS-ewkino-low-$E_{\mathrm{T}}^{\mathrm{miss}}$-high-$\Delta m$ VR-SS-ewkino-low-$E_{\mathrm{T}}^{\mathrm{miss}}$-low-$\Delta m$	Same sign $\ell^{\pm}\ell^{\pm}$	$ee + \mu e$, $\mu\mu + e\mu$	$R_{\mathrm{ISR}} \in [0.7, 1.0]$, $m_{\mathrm{T}}^{\ell_1}$ and $p_{\mathrm{T}}^{\ell_2}$ removed $E_{\mathrm{T}}^{\mathrm{miss}}/H_{\mathrm{T}}^{\mathrm{lep}}$, $m_{\mathrm{T}}^{\ell_1}$ and $p_{\mathrm{T}}^{\ell_2}$ removed –
VR-DF-ewkino-high-$E_{\mathrm{T}}^{\mathrm{miss}}$ VR-DF-ewkino-low-$E_{\mathrm{T}}^{\mathrm{miss}}$-high-$\Delta m$ VR-DF-ewkino-low-$E_{\mathrm{T}}^{\mathrm{miss}}$-low-$\Delta m$	$e\mu + \mu e$	$e\mu + \mu e$	– – –

Table 5: Definition of control ("CR-" prefix) and validation ("VR-" prefix) regions used for background estimation in the electroweakino search. The preselection criteria from Table 2 and selection criteria from Table 3 are implied unless specified. Additional or modified requirements are provided with respect to the selection of the signal region indicated in the suffix of the CR or VR.

Region	SR orthogonality	Lepton Flavor	Additional requirements
CR-top-slepton-high-$E_{\mathrm{T}}^{\mathrm{miss}}$ CR-top-slepton-low-$E_{\mathrm{T}}^{\mathrm{miss}}$	$N_{b-\mathrm{jet}}^{20} \geq 1$	$ee + \mu\mu + e\mu + \mu e$	$R_{\mathrm{ISR}} \in [0.7, 1.0]$ $E_{\mathrm{T}}^{\mathrm{miss}} \in [120, 200]$
CR-tau-slepton-high-$E_{\mathrm{T}}^{\mathrm{miss}}$ CR-tau-slepton-low-$E_{\mathrm{T}}^{\mathrm{miss}}$	$m_{\tau\tau} \in [60, 120]$ GeV	$ee + \mu\mu + e\mu + \mu e$	$R_{\mathrm{ISR}} \in [0.7, 1.0]$ $R_{\mathrm{ISR}} \in [0.6, 1.0]$, $E_{\mathrm{T}}^{\mathrm{miss}} \in [120, 200]$
CR-VV-slepton-high-$E_{\mathrm{T}}^{\mathrm{miss}}$ CR-VV-slepton-low-$E_{\mathrm{T}}^{\mathrm{miss}}$	$R_{\mathrm{ISR}} \in [0.7, 0.85]$ $R_{\mathrm{ISR}} \in [0.6, 0.8]$	$ee + \mu\mu + e\mu + \mu e$	– $m_{\mathrm{T}}^{\ell_1} > 30$, $N_{\mathrm{jets}} = 1$
VR-DF-slepton-high-$E_{\mathrm{T}}^{\mathrm{miss}}$ VR-DF-slepton-low-$E_{\mathrm{T}}^{\mathrm{miss}}$	$e\mu + \mu e$	$e\mu + \mu e$	– –

Table 6: Definition of control ("CR-" prefix) and validation ("VR-" prefix) regions used for background estimation in the slepton search. The preselection criteria from Table 2 and selection criteria from Table 4 are implied unless specified. Additional or modified requirements are provided with respect to the selection of the signal region indicated in the suffix of the CR or VR.

The definitions of the CR's and VR's used in the electroweakino and slepton searches are summarised in Tables 5 and 6, respectively.

The source of background in the $1\ell 1T$ channel is dominantly combinatorial, from events containing one prompt lepton and one random track, and is collectively estimated using data.

6.1 Reducible Background in Regions with Two Leptons

The FNP lepton background arises from jets misidentified as leptons, photon conversions, or semileptonic decays of heavy-flavour hadrons. Studies based on simulated samples indicate that the latter is the dominant component in the SRs with two leptons. The contamination of FNP lepton background in the SRs is large at low values of $m_{\ell\ell}$ and m_{T2}, and decreases at the upper end of the distributions.

In the Fake Factor method, a two-lepton control sample is defined in data, where one of the leptons, labelled as ID, meets all the requirements applied to signal leptons used in the analysis, and the other lepton, labelled as anti-ID, fails one of these requirements and instead satisfies less restrictive ones. This sample is enriched in FNP lepton backgrounds and is therefore referred to as the FNP control sample. The contributions from processes with two prompt leptons in the FNP control sample are subtracted using simulated samples. MC studies indicate that the leptons in the FNP control sample arise from processes similar to those for FNP leptons passing the SR selections. The FNP lepton background prediction in a given region is obtained by applying all selection requirements of that region to the FNP control sample and scaling the observed number of events by an extrapolation factor, referred to as the fake factor.

The fake factor is measured in a data sample collected with prescaled low-p_{T} single-lepton triggers, which is dominated by multijet events with FNP leptons and is referred to as the measurement sample. A selection of $m_{\mathrm{T}}^{\ell_1} < 40$ GeV is applied to reduce the contributions from processes with prompt leptons in the measurement sample. The contributions from these processes is subtracted using MC simulation, with negligible impact on the measured fake factors.

To enrich the sample in FNP leptons similar to those contaminating the SRs, the leading jet p_{T} is required to be greater than 100 GeV. The fake factors are calculated as the ratio of ID to anti-ID leptons in the measurement sample, measured in bins of lepton p_{T}, separately for electrons and muons. The fake factors are also found to have a dependence on the number of b-tagged jets in the events. Different fake factors are therefore computed in events with > 0 and with zero b-tagged jets.

The yields predicted by the Fake Factor method are cross-checked in dedicated VRs enriched in FNP lepton backgrounds, labelled VR-SS. As summarised in Table 5, for each electroweakino SR, a VR-SS is constructed by selecting events with two leptons with the same electric charge. As the subleading lepton is found to be the FNP lepton in most cases, the VR-SS are divided into $ee + \mu e$ and $\mu\mu + e\mu$, where the left (right) lepton of each pair denotes the leading (subleading) lepton. The kinematic requirements applied to each VR-SS are mostly the same as the ones used in the corresponding SR, ensuring the FNP lepton processes are similar in the two regions. To guarantee high purity in FNP lepton background, the selection criteria designed to suppress these processes in the SRs, such as the sliding cut on the p_{T} threshold of the subleading lepton, are loosened or removed in each VR-SS. The VR-SS-ewkino-low-$E_{\mathrm{T}}^{\mathrm{miss}}$-high-$\Delta m$ and VR-SS-ewkino-high-$E_{\mathrm{T}}^{\mathrm{miss}}$ regions are also used to validate the FNP lepton background modelling in the Low-$E_{\mathrm{T}}^{\mathrm{miss}}$ and High-$E_{\mathrm{T}}^{\mathrm{miss}}$ slepton SRs. The contribution of FNP background in the VR-SS regions is typically above 93%, with the remaining backgrounds originating from VV processes with two prompt leptons of the same electric charge. The signal contamination is at most 14%.

6.2 Irreducible Background in Regions with Two Leptons

Several CRs are defined for the electroweakino and slepton searches and are used to normalise the MC simulations of $t\bar{t}/tW$, $Z^{(*)}/\gamma^{*}(\rightarrow \tau\tau)$ + jets and WW/WZ background processes to the data in a simultaneous fit also including the SRs, described in Section 8. The event rates in the SRs are predicted by

extrapolating from the CRs using the simulated MC distributions. This extrapolation is validated using events in dedicated VRs, which are not used to constrain the fit and are orthogonal in selection to the CRs and SRs.

The CRs are designed to be statistically disjoint from the SRs, to be enriched in a particular background process, to have minimal contamination from the signals considered, and to exhibit kinematic properties similar to the SRs. The CRs labelled as CR-top are defined by selecting events with at least one b-tagged jet. The CR-top regions have purities ranging from 83% to 94% in processes with top quarks and are used to constrain the normalisation of the $t\bar{t}$ and tW processes with dilepton final states. The CR-tau regions, samples enriched in the $Z^{(*)}/\gamma^*(\rightarrow \tau\tau)$ + jets process with purities of at least 82%, are constructed by selecting events satisfying $m_{\tau\tau} \in [60, 120]$ GeV. Finally, the R_{ISR} selection used to define the SRs is modified to construct CRs enriched in WW and WZ processes, denoted CR-VV. These samples consist of approximately $41 - 45\%$ VV events.

The $t\bar{t}/tW$, WW/WZ and $Z^{(*)}/\gamma^*(\rightarrow \tau\tau)$ + jets processes containing two prompt leptons all yield same-flavour lepton pairs (ee and $\mu\mu$) at the same rate as for different-flavour pairs ($e\mu$ and μe, where the first lepton is the leading lepton). This feature is used to enhance the statistical constraining power of the CRs, by selecting events with all possible flavour assignments (ee, $\mu\mu$, $e\mu$, and μe). It is also used to define additional VRs, denoted VR-DF. One VR-DF is defined for each 2ℓ SR by requiring two different-flavour leptons ($e\mu$ and μe), but otherwise keeping the same kinematic selections as the corresponding SR. The relative fractions of each background process are similar in the SR and the corresponding VR-DF. The signal contamination in the VR-DF regions is at most 16%, originating from $\widetilde{\chi}_1^+\widetilde{\chi}_1^-$ or $\widetilde{\chi}_2^0\widetilde{\chi}_1^\pm$ Higgsino events decaying fully leptonically.

In the search for electroweakinos, six single-bin CRs are defined as summarised in Table 5. Three CRs, labelled high-$E_{\text{T}}^{\text{miss}}$, employ a $E_{\text{T}}^{\text{miss}} > 200$ GeV selection and are used to constrain the normalisation of $t\bar{t}/tW$, WW/WZ and $Z^{(*)}/\gamma^*(\rightarrow \tau\tau)$ + jets backgrounds in the High-$E_{\text{T}}^{\text{miss}}$ electroweakino SR. To minimise the impact of the mismodelling of the trigger efficiency in MC, three additional CRs, labelled low-$E_{\text{T}}^{\text{miss}}$-high-$\Delta m$, are defined by selecting events with $E_{\text{T}}^{\text{miss}} \in [120, 200]$ GeV. These CRs are used to normalise the same background processes in the Low-$E_{\text{T}}^{\text{miss}}$, high-$\Delta m$ SR. Events with FNP leptons entering the CRs are suppressed using the same sliding cut on $p_{\text{T}}^{\ell_2}$ as the corresponding SRs.

The dominant source of irreducible background in the Low-$E_{\text{T}}^{\text{miss}}$, low-$\Delta m$ SR originates from the $Z^{(*)}/\gamma^*(\rightarrow \tau\tau)$ + jets process. It is difficult to construct a dedicated CR with enough events to constrain the normalisation of the $Z^{(*)}/\gamma^*(\rightarrow \tau\tau)$ + jets background in the Low-$E_{\text{T}}^{\text{miss}}$, low-$\Delta m$ SR. The CR-tau-ewkino-low-$E_{\text{T}}^{\text{miss}}$-high-$\Delta m$ is therefore used for this purpose. The extrapolation from CR-tau-ewkino-low-$E_{\text{T}}^{\text{miss}}$-high-$\Delta m$ to the Low-$E_{\text{T}}^{\text{miss}}$, low-$\Delta m$ SR is tested in an additional VR, labelled VR-tau-ewkino-low-$E_{\text{T}}^{\text{miss}}$-low-$\Delta m$, defined by selecting events with $m_{\tau\tau} \in [60, 120]$ GeV, but otherwise applying the same kinematic selections as the Low-$E_{\text{T}}^{\text{miss}}$, low-$\Delta m$ SR, as summarised in Table 5.

Six CRs are used to normalise the $t\bar{t}/tW$, WW/WZ and $Z^{(*)}/\gamma^*(\rightarrow \tau\tau)$ + jets background processes entering the Low- and High-$E_{\text{T}}^{\text{miss}}$ slepton SRs, as summarised in Table 6. The CRs used in the search for sleptons follow a similar design to the CRs used in the search for electroweakinos. One notable difference is the sliding cut on the $p_{\text{T}}^{\ell_2}$ threshold, which is chosen to match the the requirements used in the slepton SRs and therefore depends on m_{T2}.

6.3 Background in the $1\ell 1T$ Channel

The background in the $1\ell 1T$ SR is suppressed by requiring that the selected track be associated to a reconstructed lepton candidate. Simulation studies show that this background is dominated by events with one prompt lepton and one track from hadrons, nonprompt leptons, or reconstructed from spurious hits and therefore not originating from a charged particle. The MC samples used to model SM processes with two prompt leptons contribute negligibly in the $1\ell 1T$ SR.

The amount of background in the $1\ell 1T$ SR is estimated using a data-driven procedure. A control sample is defined in data with events that pass the same selection criteria as the $1\ell 1T$ SR. Instead of selecting OS events with one lepton and one track, the lepton and the track in the control sample are required to have the same electric charge (SS). The signal contamination in the SS control sample is negligible. The data in the SS sample are directly used as the estimate of the background in the $1\ell 1T$ SR. The background estimate assumes that the background events are produced with equal rates for OS and SS events. This is expected to be the case because the track is randomly selected and its electric charge is not correlated to the charge of the prompt lepton. This assumption is tested in simulation and data, and a systematic uncertainty is assigned to cover any bias in the background estimate.

The assumption that OS and SS background events are produced with equal rates is tested using W+ jets simulated events passing the $1\ell 1T$ kinematic selections. The ratio of OS and SS W+ jets events was found to be compatible with one, with a statistical uncertainty of 12% determined by the size of the MC sample. A VR, denoted VR-$1\ell 1T$, is constructed to test the assumption using data. The VR-$1\ell 1T$ is designed using the the same kinematic selections as the $1\ell 1T$ SR, except $\Delta\phi(\text{lep}, \mathbf{p}_{\text{T}}^{\text{miss}}) > 1.5$ is required to ensure that the samples are disjoint. The upper bound on $\Delta R_{\ell\text{track}}$ used in the SR is removed to reduce the signal contamination, and the $E_{\text{T}}^{\text{miss}}/H_{\text{T}}^{\text{lep}}$ requirement is loosened to $E_{\text{T}}^{\text{miss}}/H_{\text{T}}^{\text{lep}} > 15$ to increase the number of events in the validation region. The kinematic distributions of the SS and OS data events in the VR-$1\ell 1T$ are compared and found to agree.

7 Systematic Uncertainties

Systematic uncertainties are evaluated for all background processes and signal samples. As the predictions for the main SM background processes modelled via MC simulation are normalised to data in dedicated control regions, the systematic uncertainties only affect the extrapolation to the signal regions in these cases.

Figure 5 illustrates the dominant classes of uncertainties in the expected background yields in the exclusive electroweakino and slepton SRs. The main sources of experimental uncertainty affect the FNP background predictions obtained with the Fake Factor method. These systematic uncertainties stem from the size of the samples used to measure the fake factors, and from differences in the event and lepton kinematics between the measurement region and the signal regions. Moreover, additional uncertainties are computed as the differences between the FNP background predictions, and observed data in the VR-SS regions. The uncertainties associated to the subtraction in the Fake Factor measurement regions of processes involving prompt leptons, estimated from simulation, are instead found to be negligible.

Other sources of significant experimental systematic uncertainties are the jet energy scale (JES) and resolution (JER). The jet uncertainties are derived as a function of p_{T} and η of the jet, as well as of the pile-up conditions and the jet flavour composition of the selected jet sample. They are determined

using a combination of simulated samples and studies of data, such as measurements of the jet balance in dijet, Z+jet and γ+jet events [104]. The systematic uncertainties related to the modelling of $E_{\mathrm{T}}^{\mathrm{miss}}$ in the simulation are estimated by propagating the uncertainties on the energy and momentum scale of each of the objects entering the calculation, as well as the uncertainties on the soft term resolution and scale [98].

The reconstruction, identification and isolation efficiencies for low-p_{T} leptons, as well as the momentum resolution and scale, are measured and calibrated following similar methods as those employed for higher-p_{T} electrons [88, 105] and muons [87]. The associated systematic uncertainties are in general found to be small.

The MC samples simulating the dominant background processes, $t\bar{t}/tW$, $Z^{(*)}/\gamma^{*}(\rightarrow \tau\tau)$ + jets and VV, are also affected by different sources of theoretical modelling uncertainty. The uncertainties related to the choice of QCD renormalisation and factorisation scales are assessed by varying the corresponding generator parameters up and down by a factor of two around their nominal values. Uncertainties in the resummation scale and the matching scale between matrix elements and parton shower for the $Z^{(*)}/\gamma^{*}(\rightarrow \tau\tau)$ + jets samples are evaluated by varying up and down by a factor of two the corresponding parameters in Sherpa. The uncertainties associated to the choice of the PDF set, NNPDF [48, 67], and in the strong coupling constant, α_s, are also considered.

As discussed in Sec. 6, the background predictions in the $1\ell 1T$ SR, selecting OS lepton-track pairs, are extracted from a SS data control sample. Two different types of systematic uncertainty are associated to the OS-SS extrapolation. For $m_{\ell\mathrm{track}} < 2$ GeV values, the main background contribution originates from low-mass OS resonances. A 30% uncertainty is assigned based on a fit to the OS/SS ratio as a function of $E_{\mathrm{T}}^{\mathrm{miss}}$ in the $\Delta\phi(\mathrm{lep}, \mathbf{p}_{\mathrm{T}}^{\mathrm{miss}}) > 1.5$ region. As the OS/SS ratio is observed to become flat for $E_{\mathrm{T}}^{\mathrm{miss}} > 200$ GeV, the uncertainty is computed as the value of the fitting function at $E_{\mathrm{T}}^{\mathrm{miss}} = 200$ GeV, summed linearly with the corresponding fit uncertainty. The $m_{\ell\mathrm{track}} > 2$ GeV region is instead mainly populated by W+ jets events, in which the correlation between the lepton and the track charge may introduce differences between the SS and OS expectations. A 12% uncertainty, extracted from W+ jets simulated events, is assigned.

Uncertainties on the expected yields for SUSY signals are estimated by varying by a factor of two the MG5_aMC@NLO parameters corresponding to the renormalisation, factorisation and CKKW-L matching scales, as well as the Pythia8 shower tune parameters. The overall uncertainties in the signal acceptance range from about 20% to 40% and depend on the SUSY particle mass splitting and the production process. Uncertainties in the signal acceptance due to PDF uncertainties are evaluated following the PDF4LHC15 recommendations [106] and amount to 15% at most for large $\widetilde{\chi}_2^0$ or $\widetilde{\ell}$ masses. Uncertainties in the shape of the $m_{\ell\ell}$ or m_{T2}^{100} signal distributions due to the sources above are found to be small, and are neglected.

Additional uncertainties are assigned to the predictions from signal simulation in the $1\ell 1T$ SR. An uncertainty in the modelling of the rate for reconstructed tracks that do not match a generated charged particle is accounted for. It is estimated by comparing the non-linear component of the per-event track multiplicity as a function of pileup, in data and simulation. Furthermore, the calibration procedure applied to MC to match the track impact parameter resolution in different data taking periods is also a source of systematic uncertainty. Finally, uncertainties are assigned to the track-lepton matching efficiency and the track isolation efficiency, as derived from the studies with $J\psi$ and Z events decaying to a lepton and a track, described in Section 4.

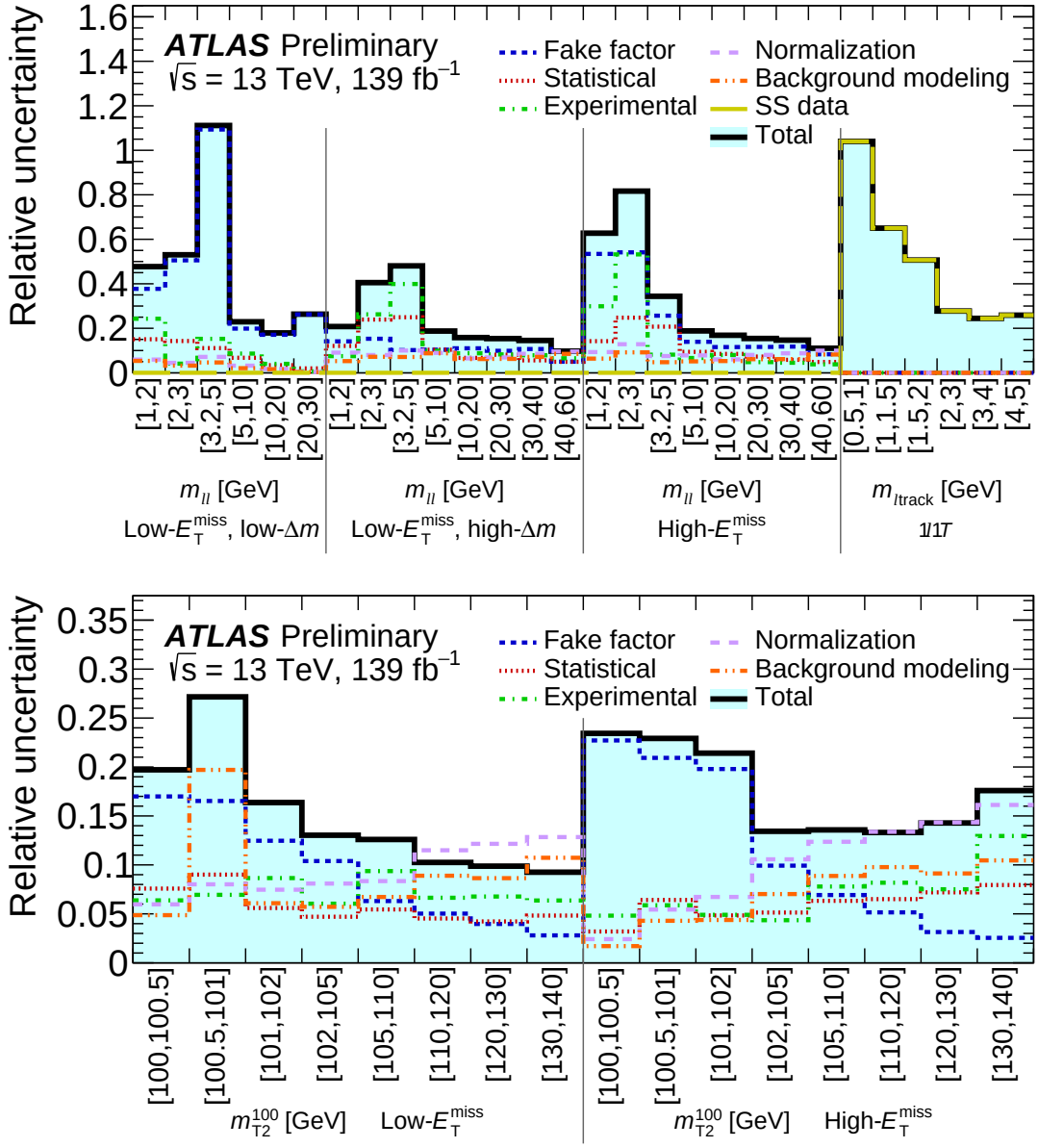

Figure 5: The relative systematic uncertainties in the background prediction as obtained from background-only fits extrapolated to the electroweakino SRs (top) and to the slepton SRs (bottom). The uncertainty on the *SS data* includes a statistical component due to the size of the SS data sample used to estimate the background in the $1\ell 1T$ SR, and a systematic component from the SS-OS extrapolation. The *Statistical* uncertainty originates from the limited size of the MC samples used to model the irreducible background contributions. The *Normalization* uncertainty arises from the use of CRs to normalise the contributions of $t\bar{t}/tW$, $Z^{(*)}/\gamma^{*}(\rightarrow \tau\tau)$ + jets and WW/WZ backgrounds. The individual uncertainties can be correlated and do not necessarily add up in quadrature to the total uncertainty.

8 Results

Data in the control regions, validation regions, and signal regions are compared to SM predictions using a profile likelihood method [107] implemented in the HistFitter package [108]. Most systematic uncertainties are treated as nuisance parameters with Gaussian constraints in the likelihood, apart from those of statistical nature, for which Poisson constraints are used. Experimental systematic uncertainties are correlated between signal and backgrounds for all regions.

8.1 Control and Validation Regions

A background-only fit is constructed using only the control regions to constrain the fit parameters. The data in the control regions CR-top, CR-tau and CR-VV are fit simultaneously in each search to constrain overall normalisation factors for the $t\bar{t}/Wt$, $Z^{(*)}/\gamma^{*}(\rightarrow \tau\tau)$ + jets, and VV background predictions. The resulting normalisation parameters are presented in Table 7.

Control Region		Normalization Parameters electroweakino	Normalization Parameters slepton
CR-top	high-$E_{\mathrm{T}}^{\mathrm{miss}}$	1.07 ± 0.04	1.03 ± 0.05
	low-$E_{\mathrm{T}}^{\mathrm{miss}}$	1.01 ± 0.02	1.00 ± 0.02
CR-tau	high-$E_{\mathrm{T}}^{\mathrm{miss}}$	0.95 ± 0.09	0.80 ± 0.13
	low-$E_{\mathrm{T}}^{\mathrm{miss}}$	0.99 ± 0.05	1.02 ± 0.06
CR-VV	high-$E_{\mathrm{T}}^{\mathrm{miss}}$	0.88 ± 0.19	0.83 ± 0.23
	low-$E_{\mathrm{T}}^{\mathrm{miss}}$	0.75 ± 0.14	0.72 ± 0.15

Table 7: Normalization factors obtained from a background-only fit of the control regions defined for electroweakino and slepton searches. The uncertainties include statistical and systematic contributions combined.

The background prediction as obtained from the background-only fit is then compared with data in the validation regions to verify the accuracy of the background modelling. Figure 6 shows a comparison of the data yields with background predictions in the VR-DF regions, binned in $m_{\ell\ell}$ and m_{T2} using the same intervals defined for the corresponding SRs. Good agreement is observed in all event selection categories, with deviations below 2σ. Examples of kinematic distributions in control and validation regions are presented in Figures 7 and 8, where good agreement between data and MC is seen in both the shape and normalisation of the discriminating variables.

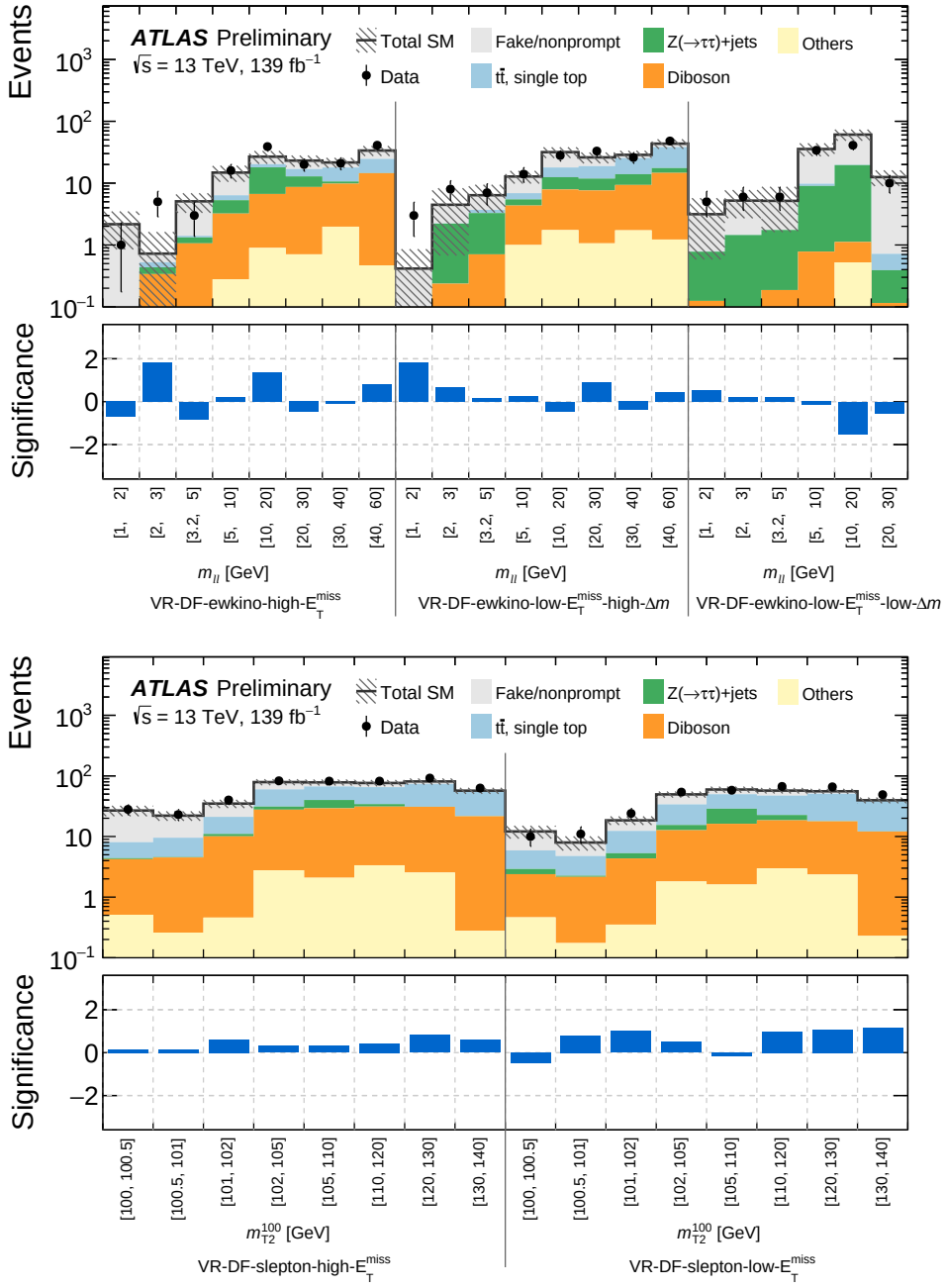

Figure 6: Comparison of observed and expected event yields in the VR-DF after a background-only fit of the control regions. The three electroweakino VR-DF are shown at the top, binned in $m_{\ell\ell}$ as the corresponding SRs. The two slepton VR-DF are shown at the bottom, binned in m_{T2} as the corresponding SRs. Uncertainties in the background estimates include both the statistical and systematic uncertainties. The bottom panel in both plots shows the significance of the difference between the expected and observed yields [102].

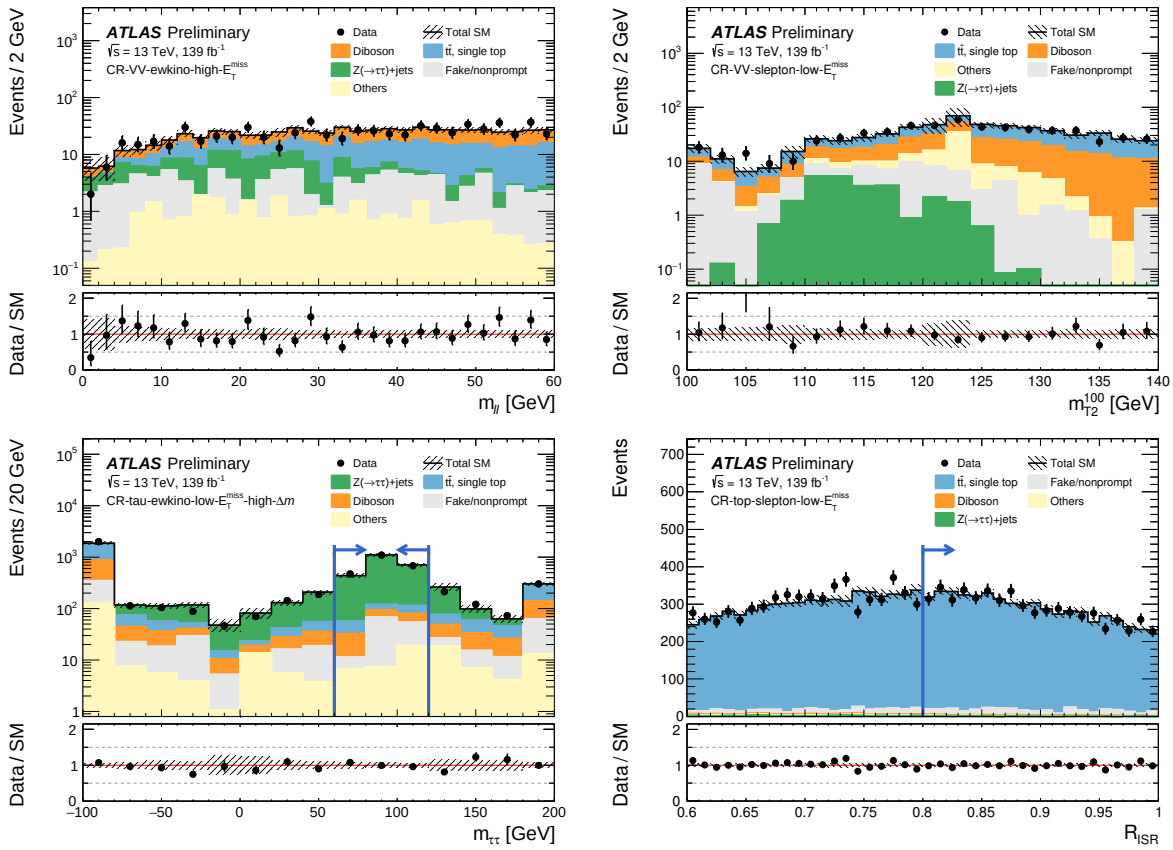

Figure 7: Examples of kinematic distributions after the background-only fit showing the data as well as the expected background in the control regions CR-VV-ewkino-high-$E_{\mathrm{T}}^{\mathrm{miss}}$ (top left), CR-VV-slepton-low-$E_{\mathrm{T}}^{\mathrm{miss}}$ (top right), CR-tau-ewkino-low-$E_{\mathrm{T}}^{\mathrm{miss}}$-high-$\Delta m$ (bottom left) and CR-top-slepton-low-$E_{\mathrm{T}}^{\mathrm{miss}}$ (bottom right). The full event selection of the corresponding regions is applied, except for the requirement that is imposed on the variable being plotted. This requirement is indicated by blue arrows in the distributions. The first (last) bin includes underflow (overflow). The uncertainty bands plotted include all statistical and systematic uncertainties.

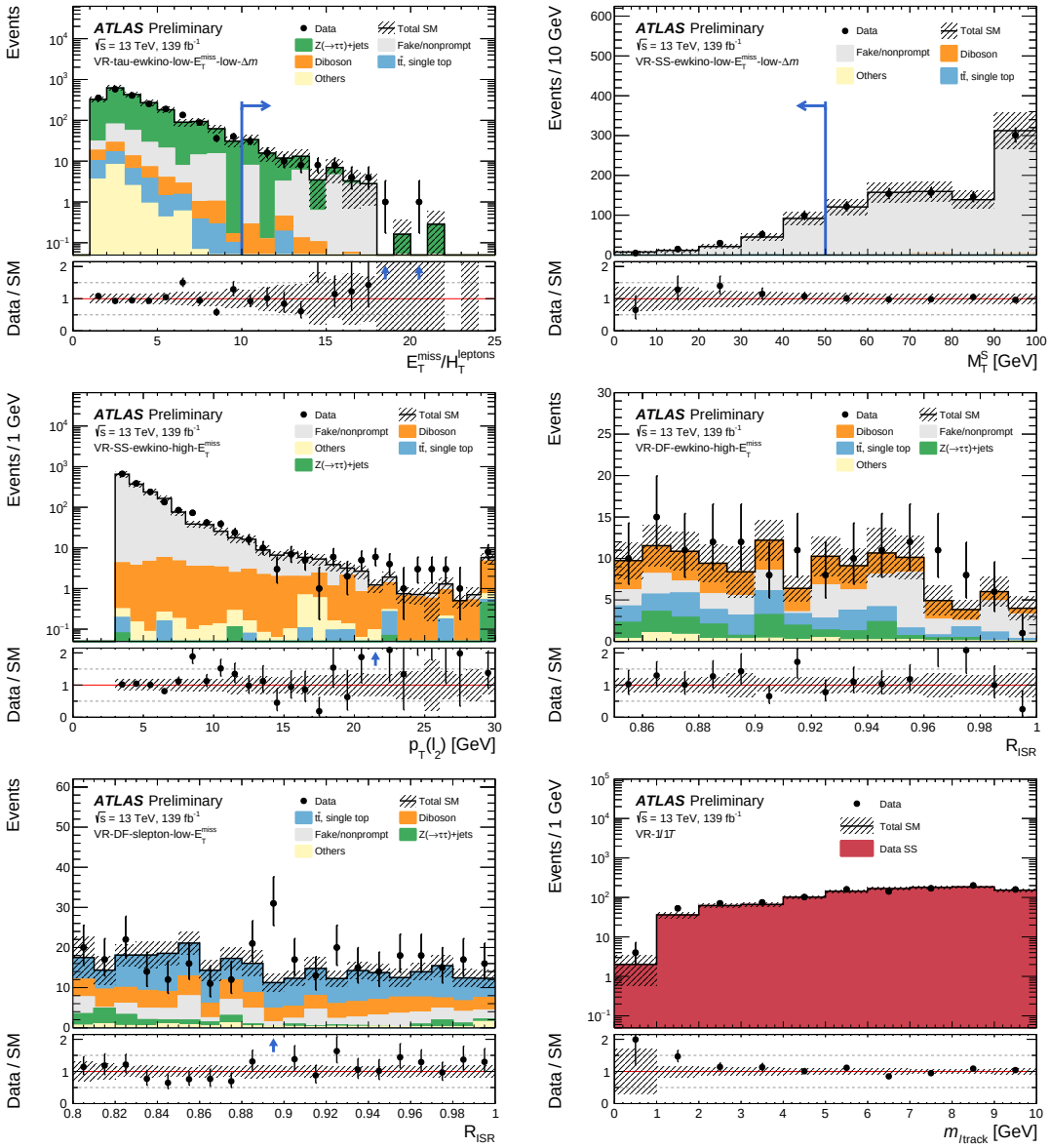

Figure 8: Examples of kinematic distributions after the background-only fit showing the data as well as the expected background in the validation regions VR-tau-ewkino-low-$E_{\mathrm{T}}^{\mathrm{miss}}$-low-$\Delta m$ (top left), VR-SS-low-$E_{\mathrm{T}}^{\mathrm{miss}}$-low-$\Delta m$ (top right), VR-SS-ewkino-high-$E_{\mathrm{T}}^{\mathrm{miss}}$ (middle left), VR-DF-ewkino-high-$E_{\mathrm{T}}^{\mathrm{miss}}$ (middle right), VR-DF-slepton-low-$E_{\mathrm{T}}^{\mathrm{miss}}$ (bottom left) and VR-1ℓ1T (bottom right). The full event selection of the corresponding regions is applied, except for the distributions at the top, where the requirement on the variable being plotted is indicated by blue arrows. The first (last) bin includes underflow (overflow). The uncertainty bands plotted include all statistical and systematic uncertainties.

8.2 Exclusive Signal Regions and Model-Dependent Interpretations

The exclusive signal regions are used to constrain specific SUSY models. An exclusion fit is defined as a background-only fit that is extended to include signal regions relevant for the model under study. All regions are fit simultaneously with a parameter of interest corresponding to the signal strength, a factor that coherently scales the signal yield across all regions. In order to assess the stability of the exclusion fit after adding the exclusive signal regions, an "SR-constrained background-only fit" is performed in which the signal strength is fixed to zero. Comparisons of the data yields with background prediction in the $m_{\ell\ell}$ and m_{T2} bins of the SRs, after the SR-constrained background-only fit, are shown in Fig. 9, with deviations $< 2\sigma$. Examples of kinematic distributions in the SRs are presented in Figures 10 and 11, where good agreement between data and the background predictions is seen in both the shape and the normalisation of the discriminating variables.

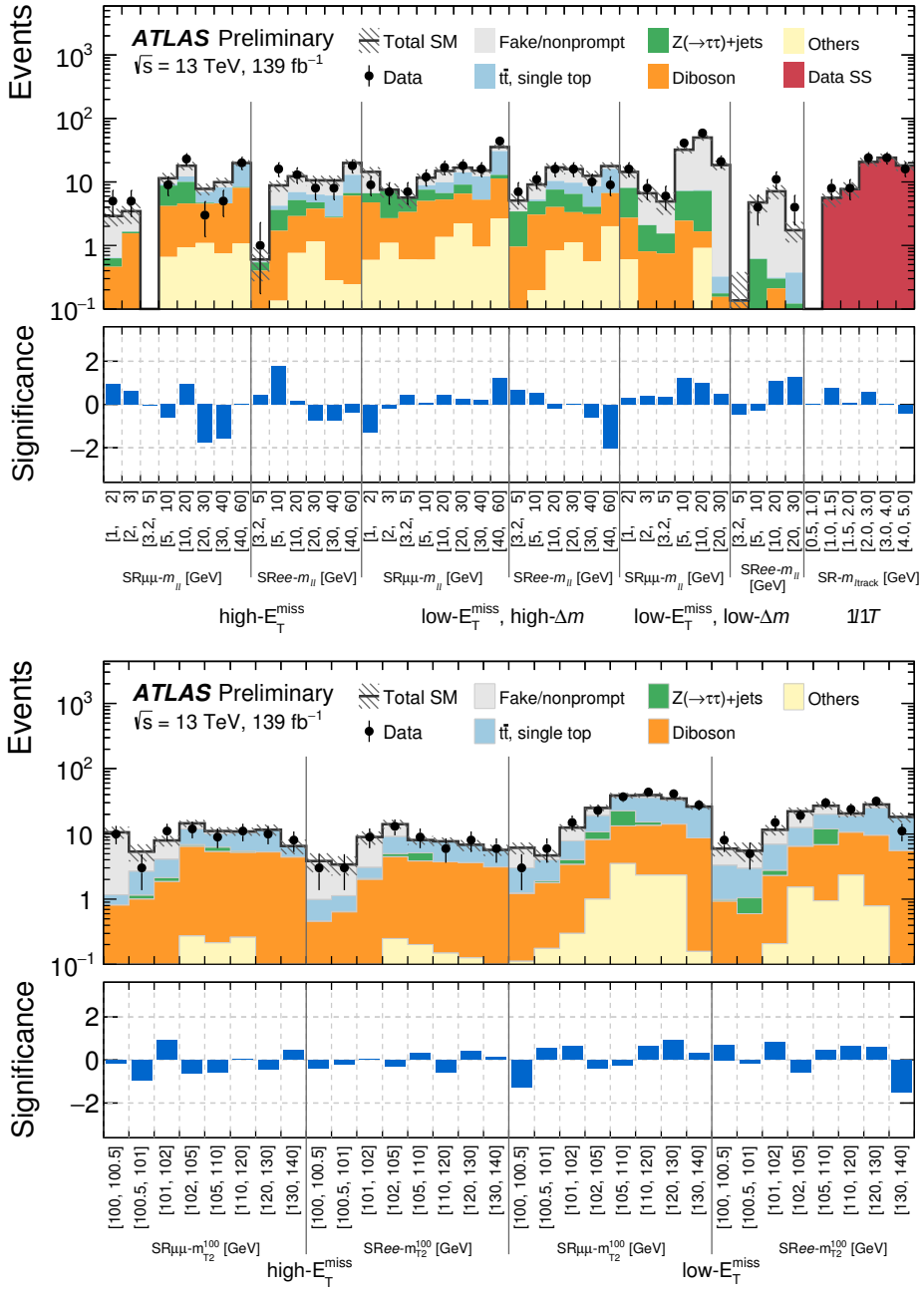

Figure 9: Comparison of observed and expected event yields in the SRs after the SR-constrained background-only fits. The SRs used for electroweakino searches recoiling against ISR are shown at the top, binned in $m_{\ell\ell}$. The SRs used for slepton searches recoiling agains ISR are shown at the bottom, binned in m_{T2}. Uncertainties in the background estimates include both the statistical and systematic uncertainties. The bottom panel in both plots shows the significance of the difference between the expected and observed yields [102].

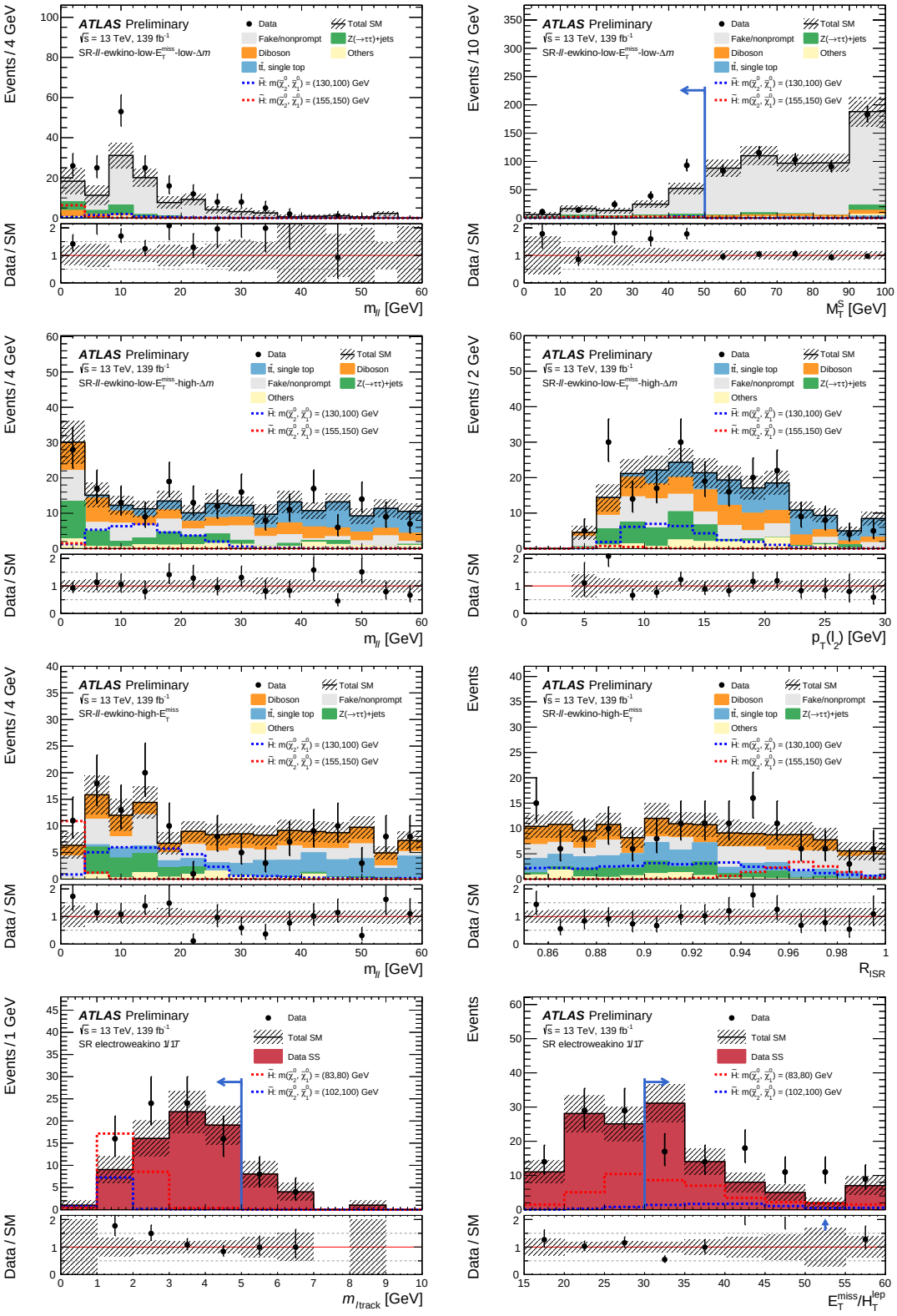

Figure 10: Examples of kinematic distributions after the background-only fits showing the data as well as the expected background in the signal regions sensitive to electroweakinos. The full event selection of the corresponding regions is applied, except for the requirement that is imposed on the variable being plotted. This requirement is indicated by blue arrows in the distributions. The first (last) bin includes underflow (overflow). The uncertainty bands plotted include all statistical and systematic uncertainties.

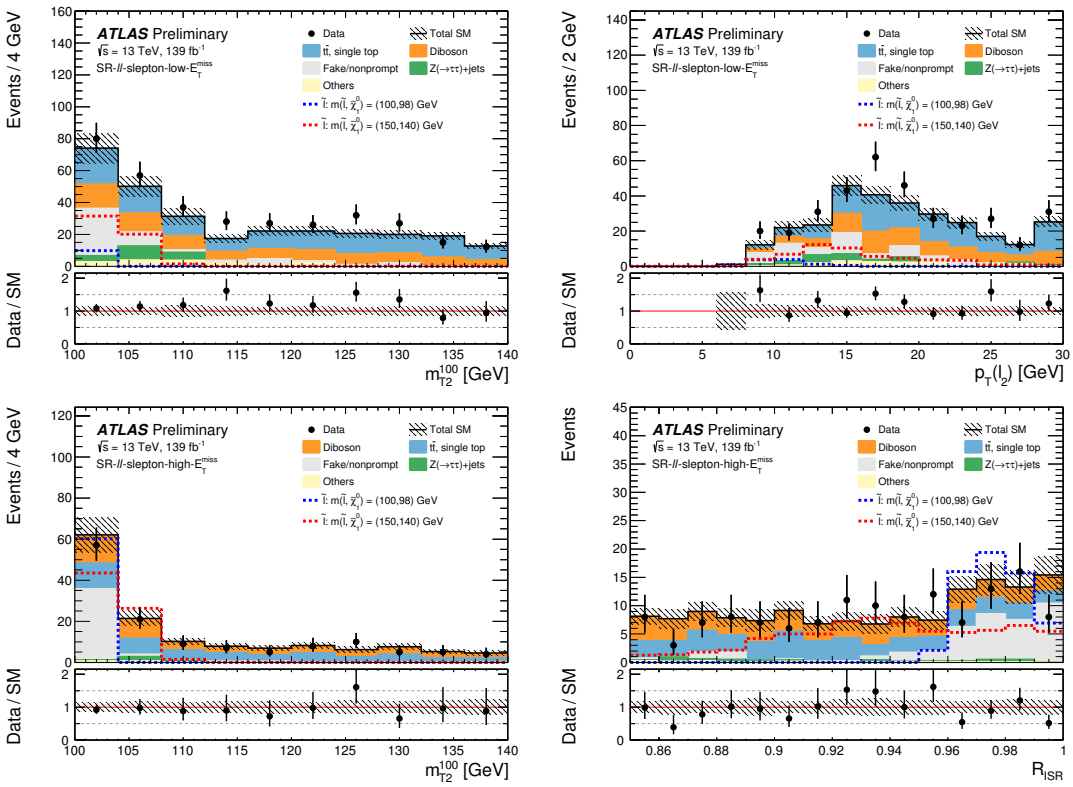

Figure 11: Examples of kinematic distributions after the SR-constrained background-only fits showing the data as well as the expected background in the signal regions sensitive to sleptons. The full event selection of the corresponding regions is applied, except for the requirement that is imposed on the variable being plotted. This requirement is indicated by blue arrows in the distributions. The first (last) bin includes underflow (overflow). The uncertainty bands plotted include all statistical and systematic uncertainties.

The CL_s prescription is used to perform hypothesis tests of specific SUSY models. The SRs defined using $m_{\ell\ell}$ are used for electroweakino models, while regions defined using m_{T2} are used for slepton models. Exclusions at 95% confidence level are presented in a 2D plane with the horizontal axis given by the mass of the $\widetilde{\chi}_2^0$, and the vertical axis defined by the difference in mass between the $\widetilde{\chi}_2^0$ and the $\widetilde{\chi}_1^0$. Particular emphasis is placed on regions of parameter space that are not excluded by LEP.

Exclusion contours for both wino and Higgsino production are shown in Fig. 12. The figures illustrate the added sensitivity provided by the $1\ell 1T$ search at small mass splittings and by the low $-E_{\mathrm{T}}^{\mathrm{miss}}$ channels at higher mass splittings. Under the assumption of wino production, electroweakino masses of up to 205 GeV for mass splittings of 5 GeV are excluded. For electroweakino masses at the edge of LEP exclusions, mass splittings from 2 GeV to 40 GeV are excluded. Assuming Higgsino production, $\widetilde{\chi}_2^0$ masses below 162 GeV are excluded for mass splittings of 10 GeV. At the LEP bounds on $m(\widetilde{\chi}_2^0)$, mass splittings from 2.6 GeV to 53 GeV are excluded.

Exclusion contours for light-flavour sleptons are shown in Fig. 13. Assuming mass-degenerate selectrons and smuons, slepton masses below 256 GeV are excluded for mass splittings of 10 GeV. For sleptons with masses just above the LEP limits, mass splittings from 590 MeV to 29 GeV are excluded. Figure 13 also shows results where only the right/left-handed selectron or smuon is produced. Right-handed selectrons extend the LEP limits only at a mass splitting of 5 GeV to 103 GeV, while left-handed selectrons are

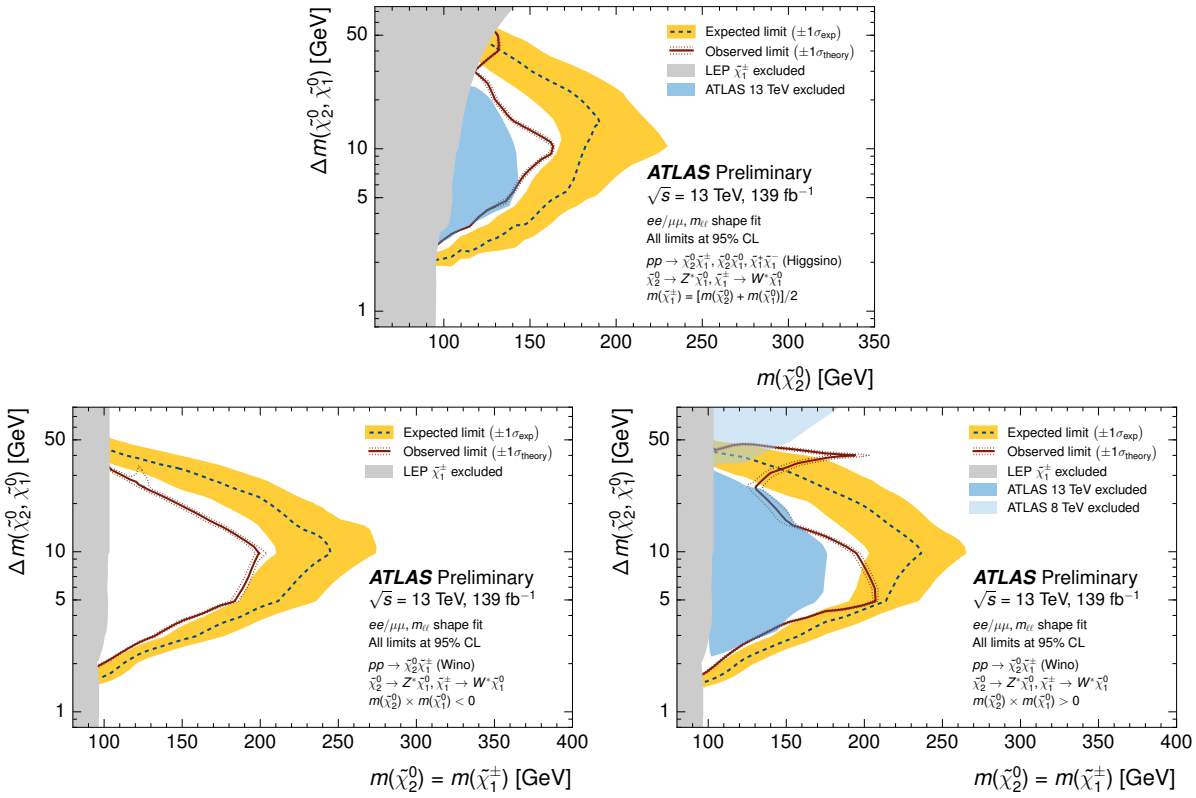

Figure 12: Expected 95% CL exclusion sensitivity (blue dashed line) with $\pm1\sigma_{\text{exp}}$ (yellow band) from experimental systematic uncertainties and observed limits (red solid line) with $\pm1\sigma_{\text{theory}}$ (dotted red line) from signal cross section uncertainties for simplified models of direct Higgsino (top) and wino (bottom) production. A fit of signals to the $m_{\ell\ell}$ spectrum is used to derive the limit, which is projected into the $\Delta m(\widetilde{\chi}_2^0, \widetilde{\chi}_1^0)$ vs. $m(\widetilde{\chi}_2^0)$ plane. For Higgsino production, the chargino $\widetilde{\chi}_1^\pm$ mass is assumed to be halfway between the $\widetilde{\chi}_2^0$ and $\widetilde{\chi}_1^0$ masses, while $m(\widetilde{\chi}_2^0) = m(\widetilde{\chi}_1^\pm)$ is assumed for the wino/bino model. For the wino/bino model, the $m_{\ell\ell}$ shape depends on the relative sign of the $\widetilde{\chi}_1^0$ and $\widetilde{\chi}_2^0$ mass parameters. The bottom left plot assumes $m(\widetilde{\chi}_1^0) \times m(\widetilde{\chi}_2^0) < 0$, while $m(\widetilde{\chi}_1^0) \times m(\widetilde{\chi}_2^0) > 0$ is assumed on the bottom right. The gray regions denote the lower chargino mass limit from LEP [27]. The blue regions indicates the limits from ATLAS Run 1 [109, 110] and Run 2 [41].

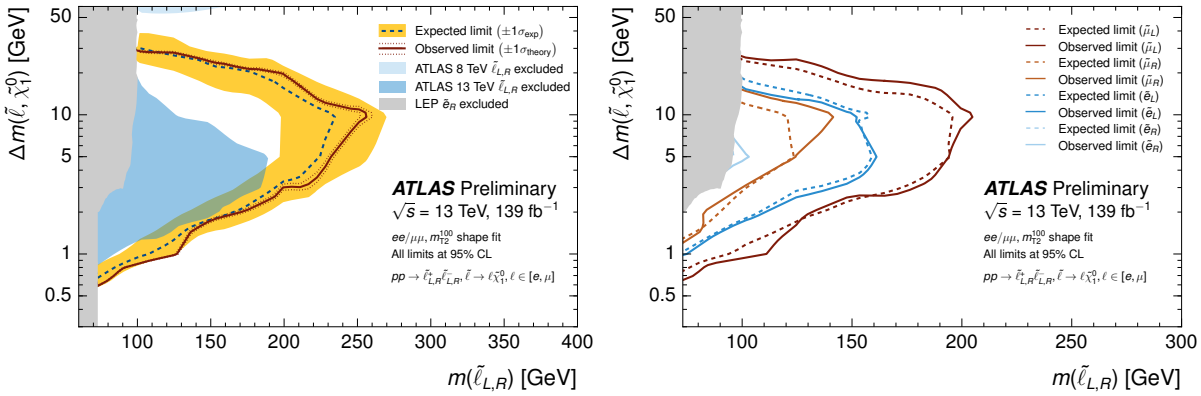

Figure 13: Expected 95% CL sensitivity (dashed lines) and observed limits (solid lines) for simplified models of direct slepton production. A fit of slepton signals to the m_{T2} spectrum is used to derive the limits, which are projected into the $\Delta m(\widetilde{\ell}, \widetilde{\chi}_1^0)$ vs. $m(\widetilde{\ell})$ plane. Slepton $\widetilde{\ell}$ refers to the scalar partners of left- and right-handed electrons and muons. The gray region is the $\widetilde{e}_R$ limit from LEP [27]. On the left, the sleptons are assumed to be fourfold mass degenerate $m(\widetilde{e}_L) = m(\widetilde{e}_R) = m(\widetilde{\mu}_L) = m(\widetilde{\mu}_R)$, the expected sensitivity (blue dashed line) is shown with with $\pm1\sigma_{\text{exp}}$ (yellow band) from experimental systematic uncertainties, the observed limit (red solid line) is shown with $\pm1\sigma_{\text{theory}}$ (dotted red line) from signal cross section uncertainties, and the blue regions are the fourfold mass degenerate slepton limits from ATLAS Run 1 [109] and Run 2 [41]. On the right, no degeneracy is assumed on the masses of the sleptons and the limits are presented separately for $\widetilde{e}_L$, $\widetilde{e}_R$, $\widetilde{\mu}_L$ and $\widetilde{\mu}_R$.

excluded up to 161 GeV for mass splittings of 5 GeV. Right-handed smuons are excluded up to 141 GeV for mass splittings of 10 GeV, while left-handed smuons are excluded up to 205 GeV for mass splittings of 10 GeV.

9 Conclusion

Results of searches for electroweak production of supersymmetric particles in models with compressed mass spectra are presented, using $\sqrt{s}$ = 13 TeV proton-proton collision data corresponding to 139 fb^{-1} collected by the ATLAS experiment at the CERN Large Hadron Collider. Events with missing transverse momentum, two same-flavour, oppositely-charged, low transverse momentum leptons, and hadronic activity from initial state radiation are selected. The data are found to be consistent with predictions from the SM. Assuming wino production constraints at 95% confidence level are placed on the minimum mass of the $\widetilde{\chi}_2^0$ at 205 GeV for a mass splitting of 5 GeV, and extend down to a mass splitting of 2 GeV at the LEP chargino mass limit. For Higgsino production, the corresponding lower limits are at 162 GeV at a mass splitting of 10 GeV, and extending down to a mass splitting of 2.6 GeV at the LEP chargino mass limit. Light-flavour sleptons are constrained to have masses above 256 GeV for a mass splitting of 10 GeV, with constraints extending down to mass splittings of 590 MeV at the LEP slepton limits.

References

[1] Yu. A. Golfand and E. P. Likhtman, *Extension of the Algebra of Poincare Group Generators and Violation of p Invariance*, JETP Lett. **13** (1971) 323, [Pisma Zh. Eksp. Teor. Fiz. **13** (1971) 452].

[2] D. V. Volkov and V. P. Akulov, *Is the Neutrino a Goldstone Particle?*, Phys. Lett. B **46** (1973) 109.

[3] J. Wess and B. Zumino, *Supergauge Transformations in Four-Dimensions*, Nucl. Phys. B **70** (1974) 39.

[4] J. Wess and B. Zumino, *Supergauge Invariant Extension of Quantum Electrodynamics*, Nucl. Phys. B **78** (1974) 1.

[5] S. Ferrara and B. Zumino, *Supergauge Invariant Yang-Mills Theories*, Nucl. Phys. B **79** (1974) 413.

[6] A. Salam and J. A. Strathdee, *Supersymmetry and Nonabelian Gauges*, Phys. Lett. B **51** (1974) 353.

[7] G. R. Farrar and P. Fayet, *Phenomenology of the Production, Decay, and Detection of New Hadronic States Associated with Supersymmetry*, Phys. Lett. B **76** (1978) 575.

[8] H. Goldberg, *Constraint on the Photino Mass from Cosmology*, Phys. Rev. Lett. **50** (1983) 1419, Erratum: *Erratum: Constraint on the Photino Mass from Cosmology*, Phys. Rev. Lett. **103** (2009) 099905.

[9] J. R. Ellis, J. S. Hagelin, D. V. Nanopoulos, K. A. Olive and M. Srednicki, *Supersymmetric Relics from the Big Bang*, Nucl. Phys. B **238** (1984) 453.

[10] J. Alwall, M.-P. Le, M. Lisanti and J. G. Wacker, *Searching for Directly Decaying Gluinos at the Tevatron*, Phys. Lett. B **666** (2008) 34, arXiv: 0803.0019 [hep-ph].

[11] J. Alwall, P. Schuster and N. Toro, *Simplified Models for a First Characterization of New Physics at the LHC*, Phys. Rev. D **79** (2009) 075020, arXiv: 0810.3921 [hep-ph].

[12] D. Alves et al., *Simplified Models for LHC New Physics Searches*, J. Phys. G **39** (2012) 105005, arXiv: 1105.2838 [hep-ph].

[13] ATLAS Collaboration, *The ATLAS Experiment at the CERN Large Hadron Collider*, JINST **3** (2008) S08003.

[14] P. Fayet, *Supersymmetry and Weak, Electromagnetic and Strong Interactions*, Phys. Lett. B **64** (1976) 159.

[15] P. Fayet, *Spontaneously Broken Supersymmetric Theories of Weak, Electromagnetic and Strong Interactions*, Phys. Lett. B **69** (1977) 489.

[16] R. Barbieri and G. F. Giudice, *Upper Bounds on Supersymmetric Particle Masses*, Nucl. Phys. B **306** (1988) 63.

[17] B. de Carlos and J. A. Casas, *One loop analysis of the electroweak breaking in supersymmetric models and the fine tuning problem*, Phys. Lett. B **309** (1993) 320, arXiv: hep-ph/9303291.

[18] R. Barbieri and D. Pappadopulo, *S-particles at their naturalness limits*, JHEP **10** (2009) 061, arXiv: 0906.4546 [hep-ph].

[19] M. Papucci, J. T. Ruderman and A. Weiler, *Natural SUSY endures*, JHEP **09** (2012) 035, arXiv: 1110.6926 [hep-ph].

[20] K. Griest and D. Seckel, *Three exceptions in the calculation of relic abundances*, Phys. Rev. D **43** (1991) 3191.

[21] J. Edsjo and P. Gondolo, *Neutralino relic density including coannihilations*, Phys. Rev. D **56** (1997) 1879, arXiv: hep-ph/9704361.

[22] S. Profumo, T. Stefaniak and L. Stephenson Haskins, *The Not-So-Well Tempered Neutralino*, Phys. Rev. D **96** (2017) 055018, arXiv: 1706.08537 [hep-ph].

[23] G. W. Bennett et al., *Final Report of the Muon E821 Anomalous Magnetic Moment Measurement at BNL*, Phys. Rev. D **73** (2006) 072003, arXiv: hep-ex/0602035 [hep-ex].

[24] A. S. Belyaev, S. F. King and P. B. Schaefers, *Muon g-2 and dark matter suggest nonuniversal gaugino masses:* $\mathbf{SU(5)} \times \mathbf{A_4}$ *case study at the LHC*, Phys. Rev. D **97** (2018) 115002, arXiv: 1801.00514 [hep-ph].

[25] C. G. Lester and D. J. Summers, *Measuring masses of semi-invisibly decaying particles pair produced at hadron colliders*, Phys. Lett. B **463** (1999) 99, arXiv: hep-ph/9906349.

[26] A. Barr, C. Lester and P. Stephens, *A variable for measuring masses at hadron colliders when missing energy is expected;* m_{T2}*: the truth behind the glamour*, J. Phys. G **29** (2003) 2343, arXiv: hep-ph/0304226.

[27] ALEPH, DELPHI, L3, OPAL Experiments, *Combined LEP Chargino Results, up to 208 GeV for low DM*, LEPSUSYWG/02-04.1, 2002, URL: http://lepsusy.web.cern.ch/lepsusy/www/inoslowdmsummer02/charginolowdm_pub.html.

[28] ALEPH, DELPHI, L3, OPAL Experiments, *Combined LEP Selectron/Smuon/Stau Results, 183-208 GeV*, LEPSUSYWG/04-01.1, 2004, URL: http://lepsusy.web.cern.ch/lepsusy/www/sleptons_summer04/slep_final.html.

[29] ALEPH Collaboration, *Search for scalar leptons in* e^+e^- *collisions at center-of-mass energies up to 209 GeV*, Phys. Lett. B **526** (2002) 206, arXiv: hep-ex/0112011.

[30] ALEPH Collaboration, *Search for charginos nearly mass degenerate with the lightest neutralino in* e^+e^- *collisions at center-of-mass energies up to 209 GeV*, Phys. Lett. B **533** (2002) 223, arXiv: hep-ex/0203020.

[31] ALEPH Collaboration, *Absolute lower limits on the masses of selectrons and sneutrinos in the MSSM*, Phys. Lett. B **544** (2002) 73, arXiv: hep-ex/0207056.

[32] ALEPH Collaboration, *Absolute mass lower limit for the lightest neutralino of the MSSM from* e^+e^- *data at* $\sqrt{s}$ *up to 209 GeV*, Phys. Lett. B **583** (2004) 247.

[33] DELPHI Collaboration, *Searches for supersymmetric particles in* e^+e^- *collisions up to 208 GeV and interpretation of the results within the MSSM*, Eur. Phys. J. C **31** (2003) 421, arXiv: hep-ex/0311019.

[34] L3 Collaboration, *Search for charginos with a small mass difference with the lightest supersymmetric particle at* $\sqrt{s} = 189$ *GeV*, Phys. Lett. B **482** (2000) 31, arXiv: hep-ex/0002043.

[35] L3 Collaboration, *Search for scalar leptons and scalar quarks at LEP*, Phys. Lett. B **580** (2004) 37, arXiv: hep-ex/0310007.

[36] OPAL Collaboration, *Search for anomalous production of dilepton events with missing transverse momentum in* e^+e^- *collisions at* $\sqrt{s} = 183$ *GeV to 209 GeV*, Eur. Phys. J. C **32** (2004) 453, arXiv: hep-ex/0309014.

[37] OPAL Collaboration, *Search for nearly mass degenerate charginos and neutralinos at LEP*, Eur. Phys. J. C **29** (2003) 479, arXiv: hep-ex/0210043.

[38] D. Egana-Ugrinovic, M. Low and J. T. Ruderman, *Charged Fermions Below 100 GeV*, JHEP **05** (2018) 012, arXiv: 1801.05432 [hep-ph].

[39] CMS Collaboration, *Search for new physics in events with two soft oppositely charged leptons and missing transverse momentum in proton-proton collisions at* $\sqrt{s} = 13$ *TeV*, Phys. Lett. B **782** (2018) 440, arXiv: 1801.01846 [hep-ex].

[40] CMS Collaboration, *Combined search for electroweak production of charginos and neutralinos in proton-proton collisions at $\sqrt{s}$ = 13 TeV*, JHEP **03** (2018) 160, arXiv: 1801.03957 [hep-ex].

[41] ATLAS Collaboration, *Search for electroweak production of supersymmetric states in scenarios with compressed mass spectra at $\sqrt{s}$ = 13 TeV with the ATLAS detector*, Phys. Rev. D **97** (2018) 052010, arXiv: 1712.08119 [hep-ex].

[42] P. Jackson and C. Rogan, *Recursive Jigsaw Reconstruction: HEP event analysis in the presence of kinematic and combinatoric ambiguities*, Phys. Rev. D **96** (2017) 112007, arXiv: 1705.10733 [hep-ph].

[43] B. Abbott et al., *Production and integration of the ATLAS Insertable B-Layer*, JINST **13** (2018) T05008, arXiv: 1803.00844 [physics.ins-det].

[44] ATLAS Collaboration, *Performance of the ATLAS trigger system in 2015*, Eur. Phys. J. C **77** (2017) 317, arXiv: 1611.09661 [hep-ex].

[45] ATLAS Collaboration, *Luminosity determination in pp collisions at $\sqrt{s}$ = 8 TeV using the ATLAS detector at the LHC*, Eur. Phys. J. C **76** (2016) 653, arXiv: 1608.03953 [hep-ex].

[46] G. Avoni et al., *The new LUCID-2 detector for luminosity measurement and monitoring in ATLAS*, JINST **13** (2018) P07017.

[47] S. D. Thomas and J. D. Wells, *Phenomenology of Massive Vectorlike Doublet Leptons*, Phys. Rev. Lett. **81** (1998) 34, arXiv: hep-ph/9804359 [hep-ph].

[48] R. D. Ball et al., *Parton distributions with LHC data*, Nucl. Phys. B **867** (2013) 244, arXiv: 1207.1303 [hep-ph].

[49] P. Artoisenet, R. Frederix, O. Mattelaer and R. Rietkerk, *Automatic spin-entangled decays of heavy resonances in Monte Carlo simulations*, JHEP **03** (2013) 015, arXiv: 1212.3460 [hep-ph].

[50] T. Sjöstrand et al., *An Introduction to PYTHIA 8.2*, Comput. Phys. Commun. **191** (2015) 159, arXiv: 1410.3012 [hep-ph].

[51] ATLAS Collaboration, *ATLAS Pythia 8 tunes to 7 TeV data*, ATL-PHYS-PUB-2014-021, 2014, URL: https://cds.cern.ch/record/1966419.

[52] L. Lönnblad and S. Prestel, *Matching tree-level matrix elements with interleaved showers*, Journal of High Energy Physics **03** (2012) 19, arXiv: 1109.4829.

[53] U. De Sanctis, T. Lari, S. Montesano and C. Troncon, *Perspectives for the detection and measurement of supersymmetry in the focus point region of mSUGRA models with the ATLAS detector at LHC*, Eur. Phys. J. C **52** (2007) 743, arXiv: 0704.2515 [hep-ex].

[54] A. Djouadi, M. M. Muhlleitner and M. Spira, *Decays of supersymmetric particles: The Program SUSY-HIT (SUspect-SdecaY-Hdecay-InTerface)*, Acta Phys. Polon. B **38** (2007) 635, arXiv: hep-ph/0609292 [hep-ph].

[55] S. Höche, F. Krauss, S. Schumann and F. Siegert, *QCD matrix elements and truncated showers*, JHEP **05** (2009) 053, arXiv: 0903.1219 [hep-ph].

[56] B. Fuks, M. Klasen, D. R. Lamprea and M. Rothering, *Gaugino production in proton-proton collisions at a center-of-mass energy of 8 TeV*, JHEP **10** (2012) 081, arXiv: 1207.2159 [hep-ph].

[57] B. Fuks, M. Klasen, D. R. Lamprea and M. Rothering, *Precision predictions for electroweak superpartner production at hadron colliders with Resummino*, Eur. Phys. J. C **73** (2013) 2480, arXiv: 1304.0790 [hep-ph].

[58] B. Fuks, M. Klasen, D. R. Lamprea and M. Rothering, *Revisiting slepton pair production at the Large Hadron Collider*, JHEP **01** (2014) 168, arXiv: 1310.2621 [hep-ph].

[59] C. Borschensky et al., *Squark and gluino production cross sections in pp collisions at* $\sqrt{s} = 13, 14, 33$ *and* 100 *TeV*, Eur. Phys. J. C **74** (2014) 3174, arXiv: 1407.5066 [hep-ph].

[60] T. Gleisberg, S. Höche, F. Krauss, M. Schönherr, S. Schumann et al., *Event generation with SHERPA 1.1*, JHEP **02** (2009) 007, arXiv: 0811.4622 [hep-ph].

[61] S. Alioli, P. Nason, C. Oleari and E. Re, *A general framework for implementing NLO calculations in shower Monte Carlo programs: the POWHEG BOX*, JHEP **06** (2010) 043, arXiv: 1002.2581 [hep-ph].

[62] ATLAS Collaboration, *Multi-Boson Simulation for* 13 *TeV ATLAS Analyses*, ATL-PHYS-PUB-2017-005, 2017, URL: https://cds.cern.ch/record/2261933.

[63] ATLAS Collaboration, *ATLAS simulation of boson plus jets processes in Run 2*, ATL-PHYS-PUB-2017-006, 2017, URL: https://cds.cern.ch/record/2261937.

[64] ATLAS Collaboration, *Studies on top-quark Monte Carlo modelling with Sherpa and MG5_aMC@NLO*, ATL-PHYS-PUB-2017-007, 2017, URL: https://cds.cern.ch/record/2261938.

[65] ATLAS Collaboration, *A study of different colour reconnection settings for Pythia8 generator using underlying event observables*, ATL-PHYS-PUB-2017-008, 2017, URL: https://cds.cern.ch/record/2262253.

[66] ATLAS Collaboration, *Modelling of the* $t\bar{t}H$ *and* $t\bar{t}V(V = W, Z)$ *processes for* $\sqrt{s} = 13$ *TeV ATLAS analyses*, ATL-PHYS-PUB-2016-005, 2016, URL: https://cds.cern.ch/record/2120826.

[67] R. D. Ball et al., *Parton distributions for the LHC Run II*, JHEP **04** (2015) 040, arXiv: 1410.8849 [hep-ph].

[68] C. Anastasiou, L. J. Dixon, K. Melnikov and F. Petriello, *High precision QCD at hadron colliders: Electroweak gauge boson rapidity distributions at NNLO*, Phys. Rev. D **69** (2004) 094008, arXiv: hep-ph/0312266.

[69] J. Pumplin et al., *New generation of parton distributions with uncertainties from global QCD analysis*, JHEP **07** (2002) 012, arXiv: hep-ph/0201195.

[70] D. de Florian et al., *Handbook of LHC Higgs Cross Sections: 4. Deciphering the Nature of the Higgs Sector*, CERN-2017-002-M (2016), arXiv: 1610.07922 [hep-ph].

[71] M. Cacciari, M. Czakon, M. Mangano, A. Mitov and P. Nason, *Top-pair production at hadron colliders with next-to-next-to-leading logarithmic soft-gluon resummation*, Phys. Lett. B **710** (2012) 612, arXiv: 1111.5869 [hep-ph].

[72] M. Czakon and A. Mitov, *NNLO corrections to top-pair production at hadron colliders: the all-fermionic scattering channels*, JHEP **12** (2012) 054, arXiv: 1207.0236 [hep-ph].

[73] M. Czakon and A. Mitov, *NNLO corrections to top pair production at hadron colliders: the quark-gluon reaction*, JHEP **01** (2013) 080, arXiv: 1210.6832 [hep-ph].

[74] M. Czakon, P. Fiedler and A. Mitov, *Total Top-Quark Pair-Production Cross Section at Hadron Colliders Through* $O(\alpha_S^4)$, Phys. Rev. Lett. **110** (2013) 252004, arXiv: 1303.6254 [hep-ph].

[75] M. Czakon and A. Mitov, *Top++: A Program for the Calculation of the Top-Pair Cross-Section at Hadron Colliders*, Comput. Phys. Commun. **185** (2014) 2930, arXiv: 1112.5675 [hep-ph].

[76] N. Kidonakis, *NNLL resummation for s-channel single top quark production*, Phys. Rev. D **81** (2010) 054028, arXiv: 1001.5034 [hep-ph].

[77] N. Kidonakis, *Next-to-next-to-leading-order collinear and soft gluon corrections for t-channel single top quark production*, Phys. Rev. D **83** (2011) 091503, arXiv: 1103.2792 [hep-ph].

[78] R. Frederix, E. Re and P. Torrielli, *Single-top t-channel hadroproduction in the four-flavour scheme with POWHEG and aMC@NLO*, JHEP **09** (2012) 130, arXiv: 1207.5391 [hep-ph].

[79] N. Kidonakis, *Two-loop soft anomalous dimensions for single top quark associated production with a W- or H-*, Phys. Rev. D **82** (2010) 054018, arXiv: 1005.4451 [hep-ph].

[80] J. Alwall, R. Frederix, S. Frixione, V. Hirschi, F. Maltoni et al., *The automated computation of tree-level and next-to-leading order differential cross sections, and their matching to parton shower simulations*, JHEP **07** (2014) 079, arXiv: 1405.0301 [hep-ph].

[81] ATLAS Collaboration, *The Pythia 8 A3 tune description of ATLAS minimum bias and inelastic measurements incorporating the Donnachie–Landshoff diffractive model*, ATL-PHYS-PUB-2016-017, 2016, URL: https://cds.cern.ch/record/2206965.

[82] A. D. Martin, W. Stirling, R. S. Thorne and G. Watt, *Parton distributions for the LHC*, Eur. Phys. J. C **63** (2009) 189, arXiv: 0901.0002 [hep-ph].

[83] ATLAS Collaboration, *The ATLAS Simulation Infrastructure*, Eur. Phys. J. C **70** (2010) 823, arXiv: 1005.4568 [physics.ins-det].

[84] S. Agostinelli et al., *GEANT4: A Simulation toolkit*, Nucl. Instrum. Meth. A **506** (2003) 250.

[85] D. J. Lange, *The EvtGen particle decay simulation package*, Nucl. Instrum. Meth. A **462** (2001) 152.

[86] ATLAS Collaboration, *Characterisation and mitigation of beam-induced backgrounds observed in the ATLAS detector during the 2011 proton–proton run*, JINST **8** (2013) P07004, arXiv: 1303.0223 [hep-ex].

[87] ATLAS Collaboration, *Muon reconstruction performance of the ATLAS detector in proton–proton collision data at* $\sqrt{s} = 13$ *TeV*, Eur. Phys. J. C **76** (2016) 292, arXiv: 1603.05598 [hep-ex].

[88] M. Aaboud et al., *Electron reconstruction and identification in the ATLAS experiment using the 2015 and 2016 LHC proton-proton collision data at* $\sqrt{s} = 13$ *TeV*, Submitted to: Eur. Phys. J. (2019), arXiv: 1902.04655 [physics.ins-det].

[89] ATLAS Collaboration, *Topological cell clustering in the ATLAS calorimeters and its performance in LHC Run 1*, Eur. Phys. J. C **77** (2017) 490, arXiv: 1603.02934 [hep-ex].

[90] M. Cacciari, G. P. Salam and G. Soyez, *The anti-k_t jet clustering algorithm*, JHEP **04** (2008) 063, arXiv: 0802.1189 [hep-ph].

[91] M. Cacciari, G. P. Salam and G. Soyez, *FastJet User Manual*, Eur. Phys. J. C **72** (2012) 1896, arXiv: 1111.6097 [hep-ph].

[92] ATLAS Collaboration, *Jet energy scale measurements and their systematic uncertainties in proton–proton collisions at* $\sqrt{s} = 13$ *TeV with the ATLAS detector*, Phys. Rev. D **96** (2017) 072002, arXiv: 1703.09665 [hep-ex].

[93] ATLAS Collaboration, *Performance of pile-up mitigation techniques for jets in pp collisions at* $\sqrt{s} = 8$ *TeV using the ATLAS detector*, Eur. Phys. J. C **76** (2016) 581, arXiv: 1510.03823 [hep-ex].

[94] ATLAS Collaboration, *Performance of b-jet identification in the ATLAS experiment*, JINST **11** (2016) P04008, arXiv: 1512.01094 [hep-ex].

[95] ATLAS Collaboration, *Optimisation of the ATLAS b-tagging performance for the 2016 LHC Run*, ATL-PHYS-PUB-2016-012, 2016, URL: https://cds.cern.ch/record/2160731.

[96] ATLAS Collaboration, *Track Reconstruction Performance of the ATLAS Inner Detector at* $\sqrt{s}$ = 13 *TeV*, ATL-PHYS-PUB-2015-018, 2015, URL: https://cds.cern.ch/record/2037683.

[97] ATLAS Collaboration, *Measurement of the photon identification efficiencies with the ATLAS detector using LHC Run 2 data collected in 2015 and 2016*, Eur. Phys. J. **C79** (2019) 205, arXiv: 1810.05087 [hep-ex].

[98] ATLAS Collaboration, E_T^{miss} *performance in the ATLAS detector using 2015–2016 LHC pp collisions*, ATLAS-CONF-2018-023, 2018, URL: https://cds.cern.ch/record/2625233.

[99] Z. Han, G. D. Kribs, A. Martin and A. Menon, *Hunting quasidegenerate Higgsinos*, Phys. Rev. D **89** (2014) 075007, arXiv: 1401.1235 [hep-ph].

[100] H. Baer, A. Mustafayev and X. Tata, *Monojet plus soft dilepton signal from light higgsino pair production at LHC14*, Phys. Rev. D **90** (2014) 115007, arXiv: 1409.7058 [hep-ph].

[101] A. Barr and J. Scoville, *A boost for the EW SUSY hunt: monojet-like search for compressed sleptons at LHC14 with 100* fb^{-1}, JHEP **04** (2015) 147, arXiv: 1501.02511 [hep-ph].

[102] R. D. Cousins, J. T. Linnemann and J. Tucker, *Evaluation of three methods for calculating statistical significance when incorporating a systematic uncertainty into a test of the background-only hypothesis for a Poisson process*, Nucl. Instrum. Meth. A **595** (2008) 480, arXiv: physics/0702156 [physics.data-an].

[103] ATLAS Collaboration, *Observation and measurement of Higgs boson decays to* WW^* *with the ATLAS detector*, Phys. Rev. D **92** (2015) 012006, arXiv: 1412.2641 [hep-ex].

[104] ATLAS Collaboration, *Jet Calibration and Systematic Uncertainties for Jets Reconstructed in the ATLAS Detector at* $\sqrt{s}$ = 13 *TeV*, ATL-PHYS-PUB-2015-015, 2015, URL: https://cds.cern.ch/record/2037613.

[105] ATLAS Collaboration, *Electron reconstruction and identification in the ATLAS experiment using the 2015 and 2016 LHC proton–proton collision data at* $\sqrt{s}$ = 13 *TeV*, Eur. Phys. J. (2019), arXiv: 1902.04655 [hep-ex].

[106] J. Butterworth et al., *PDF4LHC recommendations for LHC Run II*, J. Phys. G **43** (2016) 023001, arXiv: 1510.03865 [hep-ph].

[107] G. Cowan, K. Cranmer, E. Gross and O. Vitells, *Asymptotic formulae for likelihood-based tests of new physics*, Eur. Phys. J. C **71** (2011) 1554, arXiv: 1007.1727 [physics.data-an], Erratum: Eur. Phys. J. C **73** (2013) 2501.

[108] M. Baak et al., *HistFitter software framework for statistical data analysis*, Eur. Phys. J. C **75** (2015) 153, arXiv: 1410.1280 [hep-ex].

[109] ATLAS Collaboration, *Search for direct production of charginos, neutralinos and sleptons in final states with two leptons and missing transverse momentum in pp collisions at* $\sqrt{s}$ = 8 *TeV with the ATLAS detector*, JHEP **05** (2014) 071, arXiv: 1403.5294 [hep-ex].

[110] ATLAS Collaboration, *Search for direct production of charginos and neutralinos in events with three leptons and missing transverse momentum in $\sqrt{s} = 8$ TeV pp collisions with the ATLAS detector*, JHEP **04** (2014) 169, arXiv: 1402.7029 [hep-ex].